

# ZIPG-SK: A NOVEL KNOCKOFF-BASED APPROACH FOR VARIABLE SELECTION IN MULTI-SOURCE COUNT DATA

Shan Tang<sup>1\*</sup>, Shanjun Mao<sup>1\*</sup>, Shourong Ma<sup>1†</sup>, Falong Tan<sup>1†</sup>  
<sup>1</sup> Department of Statistics, Hunan University, 410006, Changsha, China

December 2, 2024

## ABSTRACT

**Motivation:** The rapid development of sequencing technology has generated complex, highly skewed, and zero-inflated multi-source count data. This has posed significant challenges in variable selection, which is crucial for uncovering shared disease mechanisms, such as tumor development and metabolic dysregulation.

**Results:** In this study, we propose a novel variable selection method called Zero-Inflated Poisson-Gamma based Simultaneous knockoff (ZIPG-SK) for multi-source count data. To address the highly skewed and zero-inflated properties of count data, we introduce a Gaussian copula based on the ZIPG distribution for constructing knockoffs, while also incorporating the information of covariates. This method successfully detects common features related to the results in multi-source data while controlling the false discovery rate (FDR). Additionally, our proposed method effectively combines e-values to enhance power. Extensive simulations demonstrate the superiority of our method over Simultaneous Knockoff and other existing methods in processing count data, as it improves power across different scenarios. Finally, we validated the method by applying it to two real-world multi-source datasets: colorectal cancer (CRC) and type 2 diabetes (T2D). The identified variable characteristics are consistent with existing studies and provided additional insights.

**Availability:** An R package ZIPGSK implementing our method are available from <https://github.com/tsnm1/ZIPGSK>.

## 1 Introduction

With advancements in sequencing technology, vast amounts of sequencing data are now readily available from diverse sources (e.g., regions and experiments), presenting both significant opportunities and challenges in microbiology, genetics, and bioinformatics [1, 2]. However, the dimensionality of these datasets often greatly exceeds the available sample size, and only a small subset of variables are truly relevant to phenotypic outcomes, underscoring the pivotal challenge of accurate variable selection [3, 4]. For instance, a key goal of human microbiome research is to understand how microbial communities affect health and disease, with gut microbiome sequencing involving thousands of species, adding analytical complexity [5]. [6] utilized a diverse range of single-cell sequencing technologies to reveal fundamental molecular characteristics at the cellular level, with datasets typically comprising tens of thousands of genetic variables. Meanwhile, studies often require the integration of data from various origins, where information on the same set of candidate features is independently collected from different sources. For example, [7] gathered gut microbiome datasets from eight different geographic cohorts to investigate the correlation between gut microbiota and colorectal cancer (CRC). As a result, selecting variables from multi-source sequencing data has become a crucial challenge that must be addressed to advance our understanding of biological systems.

In addition to the inherent high-dimensional nature of sequencing data, these datasets, such as gut microbiome sequencing and single-cell sequencing data, are frequently represented as count data. Numerous existing methods can

\* Authors contributed equally to this research.

† Corresponding authors. Email: [falongtan@hnu.edu.cn](mailto:falongtan@hnu.edu.cn), [shourongm@hnu.edu.cn](mailto:shourongm@hnu.edu.cn)

be employed for variable selection in sequencing data. For the analysis of single-cell RNA sequencing data, a common approach involves conducting statistical tests for differential gene expression after clustering to identify marker genes [8]. For instance, [9] applied the Clustifyr package to classify cells and subsequently utilized the Wilcoxon rank sum test for differential gene detection. Alternatively, certain methods convert count data into compositional data prior to variable selection. [10] proposed a regularization approach based on a linear logarithmic contrast model that takes into account the unique characteristics of compositional data. The usefulness of this approach is demonstrated through its application in microbiome studies that explore the correlation between human body mass index (BMI) and gut microbiome composition. However, it is important to acknowledge that these methods may have certain limitations when handling count data. The former approach may suffer from the issue of double dipping [11], while the latter approach may introduce some deviation during the log-ratio transformation or when dealing with zero values, potentially leading to the loss of sequencing depth information. Besides addressing the issue of variable selection based on count data, it is essential to consider the potential influence of multiple sources. Typically, variable selection from multiple sources is approached through either pooling or intersecting [7, 12]. However, the former may introduce additional bias due to the heterogeneity of multi-source data [13], resulting in inaccurate results, while the latter may be overly strict and overlook certain potential features [14]. Consequently, more appropriate methods are necessary to effectively address variable selection in multi-source count data.

In recent years, the knockoff method has emerged as an innovative and powerful approach for variable selection, effectively controlling the false discovery rate (FDR) by constructing a set of ‘knockoff’ variables [15, 16]. This approach can also be applied to gut microbiome sequencing data. For example, [17] proposed a two-step robust knockoff filter for microbiome compositional data that effectively controls the FDR during variable selection, even in the presence of contamination. Additionally, model-X knockoff based methods have been proposed to tackle the high-dimensional challenges posed by sequencing data. However, knockoffs based on model-X knockoff methods are typically constructed using second-order information [3]. It is worth noting that count data often exhibit high skewness and an abundance of zeros, which may render the model-X knockoff method less suitable for direct count data analysis [18]. Therefore, the construction of knockoffs for count data should be carried out by other means. For example, [11] constructed knockoffs by assuming the distribution of the sequencing data, such as the negative binomial (NB) distribution, and employed Gaussian copula-based distribution fitting. However, this approach does not specifically address the issue of zero inflation commonly observed in sequencing data and lacks the capability to handle multi-source data. For multi-source data, [19] proposed a knockoff-based variable selection approach called Simultaneous knockoffs (SK), which enables the identification of shared signals from multiple independent datasets. Similarly, while this SK method, based on the model-X framework, can accommodate multi-source data, it may not be ideally suited to handle the zero inflation phenomenon of count data, making it less suitable for direct application to multi-source count data. Therefore, when using the knockoff method to analyze multi-source count data, it is crucial to appropriately assume the distribution of count data and reasonably integrate multi-source information.

In this paper, we propose a new knockoff model for multi-source count data, namely ZIPG-SK (Zero Inflated Poisson-Gamma based Simultaneous knockoff), to investigate the selection of characteristic variables related to phenotypic outcomes. When constructing knockoff variables, this method assumes a Zero-Inflated Poisson-Gamma (ZIPG) distribution [20] for count data and accounts for the influence of relevant covariates. The knockoff variables are then built based on Gaussian copula. Subsequently, the SK method is applied to integrate knockoffs of multi-source count data for variable selection. The proposed process effectively addresses the issues of high skewness and zero inflation in count data, while simultaneously integrating information from multi-source count data. Additionally, incorporating covariates associated with sequencing count data during knockoff construction can improve statistical power, while repeating the construction of knockoff variables multiple times and incorporating e-values can enhance FDR control and power [21]. This paper also presents theoretical results that are consistent with previously established findings. Through extensive simulations, we demonstrate that our model outperforms other commonly used variable selection methods for count data. Furthermore, we analyzed two real-world datasets: a microbial sequencing dataset related to CRC and a single-cell RNA sequencing dataset associated with type 2 diabetes (T2D). Many of the identified taxa and genes are corroborated by existing biological literature, and these novel findings hold potential for further experimental validation.

The remaining content of the paper is organized as follows: Section 2 presents the proposed model, including the Methods and Algorithm for ZIPG-SK. The main results from simulations and real data analysis are demonstrated in Section 3 and Section 4, respectively. Section 5 concludes the paper. A detailed description of the ZIPG-SK method, theoretical results, and additional experimental analyses of simulations and real-world data is provided in Section 5.

## 2 Materials and Methods

### 2.1 Datasets

To demonstrate the effectiveness of our proposed approach in the field of multi-source data, we investigate two typical multi-source counting datasets in this study. One dataset includes publicly available metagenomic data from six distinct gut microbiome datasets [7], while the other dataset comprises single cell RNA-seq data from patients with T2D [22]. Among them, the gut microbiome dataset was carefully preprocessed and exhibited geographical diversity. This dataset encompassed 1014 individuals, including 505 CRC patients and 509 healthy controls (HC), representing 845 unique gut microbiota species. The T2D dataset comprises transcriptome sequencing data from thousands of human islet cells obtained from healthy individuals and donors with T2D. This dataset encompasses various cell subpopulations, including  $\alpha$  cells,  $\beta$  cells, and acinar cells, along with 30415 genes. Additional details and features of both datasets are included in the supporting materials, specifically in S3.1.

### 2.2 Methods

Figure 1 illustrates the flow of the ZIPG-SK method. This section is divided into three parts. Firstly, it introduces the foundation of knockoffs in the context of multi-source multiple testing problems. Secondly, it describes the construction of knockoff count data for single sources. Finally, a basic description of the Simultaneous Knockoffs method is provided.

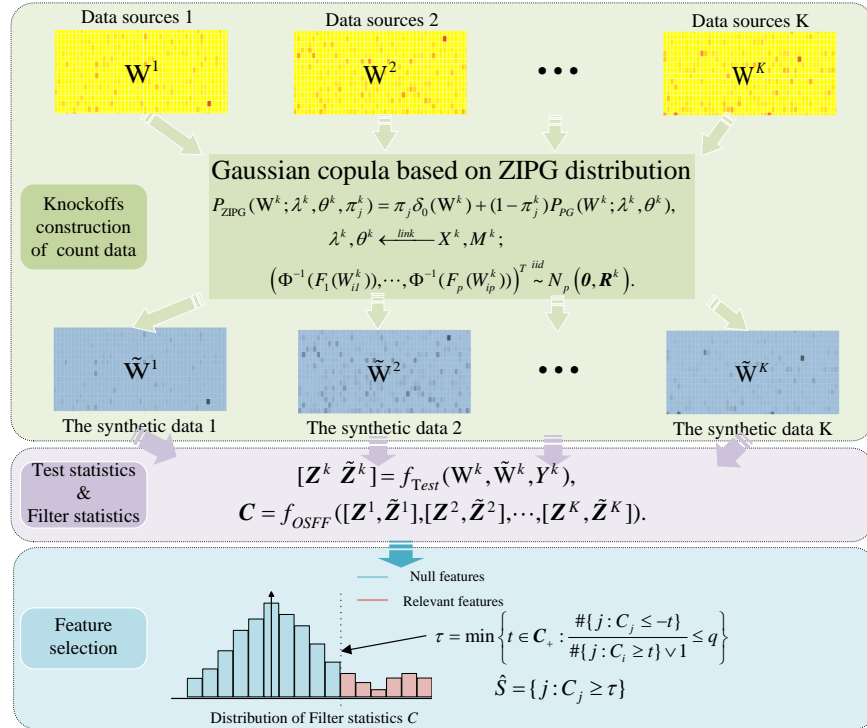


Figure 1: The flow of the ZIPG-SK. ZIPG-SK is primarily divided into three parts. The first part involves the construction of knockoff data from different sources, primarily based on the ZIPG distribution within a Gaussian copula framework. The second part focuses on the calculation of statistics, including the computation of test statistics from respective data sources and the calculation of filter statistics from multiple sources. Finally, the third part involves feature selection based on the filter statistics.

#### 2.2.1 The multiple testing for multi-source data

The ZIPG-SK method is a general framework for testing the union null hypotheses on conditional associations between candidate count features and outcomes. Assuming data from  $K$  independent experiments (sources), denote

$[K] = \{1, \dots, K\}$ . Within the  $k$ -th experiment, let  $Y_k^i$  denote the outcome variable, and  $\mathbf{W}_k^i = (W_{k1}^i, \dots, W_{kp}^i)$  represent count data associated with the  $i$ -th individual. These variables are assumed to be i.i.d. according to the distribution  $\mathcal{D}_k$ , i.e.,  $(Y_k^i, \mathbf{W}_k^i) \stackrel{iid}{\sim} \mathcal{D}_k$ ,  $i = 1, \dots, n_k$ . In our setting, the  $\mathbf{Y}_k = (Y_k^1, \dots, Y_k^{n_k})^T$  can be binary variable.

Refer to [19], and define  $H_{0,kj}$ ,  $j \in [p]$  as the null hypothesis indicating that the feature  $\mathbf{W}_{kj} = (W_{kj}^1, \dots, W_{kj}^{n_k})^T$  is not associated with  $\mathbf{Y}_k$  in the  $k$ -th experiment, i.e.,

$$H_{0,kj} : \mathbf{W}_{kj} \perp \mathbf{Y}_k | \mathbf{W}_{k,-j}$$

where  $\mathbf{W}_{k,-j} := \{\mathbf{W}_{k1}, \dots, \mathbf{W}_{kp}\} \setminus \mathbf{W}_{kj}$ . Denote  $\mathcal{H}_k = \{j \in [p] : H_{0,kj} \text{ is true}\}$ . Instead of testing the null hypotheses  $H_{0,kj}$ , our interest here is to test the union null hypotheses

$$H_{0j} = \cup_{k=1}^K H_{0,kj}, \text{ for } j \in [p]. \quad (1)$$

Define  $\mathcal{S} = \{j \in [p] : H_{0j} \text{ is false}\}$  and  $\mathcal{H} = \mathcal{S}^c = \cup_{k=1}^K \mathcal{H}_k = \{j \in [p] : H_{0j} \text{ is true}\}$ . The aim is to develop a selection procedure returning a selection set  $\hat{\mathcal{S}} \in [p]$  with a controlled FDR, which is the expected false discovery proportion (FDP):

$$FDR(\hat{\mathcal{S}}) = \mathbb{E} \left[ FDP(\hat{\mathcal{S}}) \right] = \mathbb{E} \left[ \frac{|\hat{\mathcal{S}} \cap \mathcal{H}|}{|\hat{\mathcal{S}}| \vee 1} \right]. \quad (2)$$

### 2.2.2 Knockoff construction for single-source count data

The construction of knockoffs for single-source count data is based on the aforementioned null hypothesis, making it akin to synthetic null generation. Initially, assumptions about the distribution of each count feature are required. Zero-inflated Poisson (ZIP) and zero-inflated negative binomial (ZINB) models are commonly used to fit count data, such as single-cell data and gut microbiome data, yielding good results [23, 24]. However, the ZINB model rarely accounts for the perturbation of other covariates, such as clinical factors or dietary patterns in gut microbiota data. In contrast, the ZIPG distribution proposed by [20] not only addressed these limitations but also provided flexible modeling by linking mean abundance and its dispersion to different sets of covariates.

In this context, we utilize ZIPG as the assumed distribution for count variables. Subsequently, the count data can be effectively approximated by a multivariate distribution using Gaussian copula. This section is dedicated to the  $k$ -th independent experiment, focusing specifically on the construction of knockoffs for single-source count data. For the sake of clarity, we omit the subscript notation  $k$  in the following discussions.

The details are as follows:

#### 1. The null model: ZIPG specified by the Gaussian copula

This null model assumes that, after each count feature is transformed to a standard Gaussian random variable, the  $n$  individuals represent a random sample from a  $p$ -dimensional Gaussian distribution with zero means and a correlation matrix  $\mathbf{R}$ . The intuition behind this null model is that individuals sharing the same count feature belong to a homogeneous population in the  $k$ -th experiment, in which every feature's marginal count distribution is ZIPG, and the correlation structure between features is determined by the Gaussian copula.

Under the null model, it is assumed that  $W_j^i$ , feature  $j$ 's count value in individual  $i$ , independently follows the hierarchical ZIPG distribution, that is  $\mathbf{W}_j \sim ZIPG(W; \lambda_j, \theta_j, \pi_j)$ ,  $j = 1, \dots, p$ . Specifically,

$$\begin{aligned} W_j^i | U_j^i &\sim \begin{cases} 0 & \text{with probability } \pi_j \\ \text{Poisson}(\lambda_j^i U_j^i) & \text{with probability } 1 - \pi_j, \end{cases} \\ U_j^i &\sim \text{Gamma}(\theta_j^{i-1}, \theta_j^i), \end{aligned} \quad (3)$$

where  $\lambda_j^i$  represents the true abundance level for count feature  $j$  from individual  $i$ , and  $\pi_j$  denotes the zero-inflation parameter describing the probability of true zero occurrence of count feature  $j$ .  $U_j^i$  follows Gamma distribution with the same rate parameter and shape parameter  $\theta_j^{i-1}$ . In this paper,  $\lambda_j^i$  is referred as the abundance mean parameter and  $\theta_j^i$  as the abundance dispersion parameter.

Denoting  $F_j$  as the cumulative distribution function (CDF) of  $ZIPG(\lambda_j, \theta_j, \pi_j)$ , the multivariate ZIPG distribution specified by the Gaussian copula is

$$(\Phi^{-1}(F_1(W_1^i)), \dots, \Phi^{-1}(F_p(W_p^i)))^T \stackrel{iid}{\sim} N_p(\mathbf{0}, \mathbf{R}), \quad (4)$$

where  $\Phi$  is the CDF of the standard Gaussian distribution  $N(0, 1)$ , and  $N_p(0, \mathbf{R})$  is an  $p$ -dimensional Gaussian distribution with an  $p$  dimensional 0 mean vector and an  $p$ -by- $p$  correlation matrix  $\mathbf{R}$ , and  $i = 1, \dots, n$ .

## 2. Fitting the null model to real data

The null model parameters include  $\Omega = \{\lambda_j, \theta_j, \pi_j\}_{j=1}^p$  and  $\mathbf{R}$ . To further consider covariates of interest associated with count data, the following link functions are defined (ZIPG mean model and dispersion model, respectively) [20]:

$$\begin{aligned} g(\lambda_j^i) &= \beta_{j,0} + \mathbf{X}^{iT} \boldsymbol{\beta}_j + \log(M^i), \\ g^*(\theta_j^i) &= \beta_{j,0}^* + \mathbf{X}^{iT} \boldsymbol{\beta}_j^*, \end{aligned} \quad (5)$$

where  $\mathbf{X}^i \in \mathbb{R}^d$  include covariates associated with  $\lambda_j^i$ ,  $\theta_j^i$ ;  $\boldsymbol{\beta}_j = (\beta_1, \dots, \beta_d)^T$  and  $\boldsymbol{\beta}_j^* = (\beta_1^*, \dots, \beta_d^*)^T$  are regression coefficients of covariates. The  $\log(M^i)$  term in the mean model accounts for the effect of sequencing depth variation. Throughout this paper, a logarithmic link function  $g(\cdot) = g^*(\cdot) := \log(\cdot)$  is chosen to ensure  $\lambda_j^i > 0$  and  $\theta_j^i > 0$ . The fitted null model parameters include  $\Omega = (\beta_0, \boldsymbol{\beta}^T, \beta_0^*, \boldsymbol{\beta}^{*T}, \gamma)^T$  and  $\mathbf{R}$ , where  $\gamma = \log\{\pi/(1-\pi)\}$  is the logit transformation of zero-inflated parameter  $\pi$  in ZIPG model. The parameter estimation process is discussed in Section 5.1.1.

## 3. Sampling from the fitted null model

The  $n$  Gaussian vectors of  $p$  dimensions are independently sampled from the estimated  $N_p(\mathbf{0}, \hat{\mathbf{R}})$  as  $(\tilde{V}_1^i, \dots, \tilde{V}_p^i)^T$ ,  $i = 1, \dots, n$ . Subsequently, these  $n$  Gaussian vectors are converted to ZIPG count vectors as follows:

$$\tilde{\mathbf{W}}^i := \left( \hat{F}_1^{-1}(\Phi(\tilde{V}_1^i)), \dots, \hat{F}_p^{-1}(\Phi(\tilde{V}_p^i)) \right)^T, \quad i = 1, \dots, n, \quad (6)$$

which represent the  $n$  synthetic null individuals, each of which contains  $p$  variables' synthetic null counts sampled from the null model.

In summary, the real data is an  $n$ -by- $p$  count matrix  $\mathbf{W}$  with the  $n$  real individuals  $\mathbf{W}^1, \dots, \mathbf{W}^n$  as the rows, while the synthetic null data is also an  $n$ -by- $p$  count matrix  $\tilde{\mathbf{W}}$  with the  $n$  synthetic null individuals  $\tilde{\mathbf{W}}^1, \dots, \tilde{\mathbf{W}}^n$  as the rows. Note that there is no one-to-one correspondence between the real individuals and the synthetic null individuals because the synthetic null individuals are independently sampled from the null model. Therefore, the process of constructing knockoffs for single-source count data is as follows:

- Model construction: ZIPG specified by the Gaussian copula (null model);
- Model Fitting: by fitting the null model to real data for parameter estimation;
- Synthetic null generation: Sampling from the fitted null model.

### 2.2.3 Simultaneous knockoff for multi-source count data

For the individual experiment  $k \in [K]$  and based on count matrix  $\mathbf{W}_k, \tilde{\mathbf{W}}_k$ , the test statistics  $[\mathbf{Z}_k, \tilde{\mathbf{Z}}_k] \in \mathbb{R}^{2p}$  can be constructed in two ways: the one is based on Model-X knockoffs (such as glmnet or random forest [3]), and the other is based on clustering and differential expression (DE) tests [11]. The filter statistics  $\mathbf{C}_k \in \mathbb{R}^p$  can be constructed by anti-symmetric functions based on  $[\mathbf{Z}_k, \tilde{\mathbf{Z}}_k]$ . For example, the difference function and the signed max function  $f_{as}([\mathbf{Z}, \tilde{\mathbf{Z}}]) = Z_j - \tilde{Z}_j$ ,  $j \in [p]$ .

For the calculation of the filter statistics  $\mathbf{C}$  of  $K$  experiments, the One Swap Flip Sign function (OSFF) in [19] is referenced for construction:

$$\mathbf{C} = f_{OSFF}([\mathbf{Z}_1, \tilde{\mathbf{Z}}_1], \dots, [\mathbf{Z}_K, \tilde{\mathbf{Z}}_K]). \quad (7)$$

Commonly used OSFF are Direct Diff Dot product:  $\mathbf{C} = \odot_{k=1}^K (\mathbf{Z}_k - \tilde{\mathbf{Z}}_k)$ , where  $\odot$  denotes the Hadamard product. More detailed information is available in Section 5.1.2.

Using the filter statistics  $\mathbf{C}$  above, the knockoff/knockoff+ filter is applied to obtain the selection set  $\hat{S}$  or  $\hat{S}_+$  under the Simultaneous knockoff / knockoff+ procedure.

With the knockoff filter, the selection set  $\hat{S} = \{j : C_j \geq \tau\}$ , where

$$\tau = \min \left\{ t \in \mathcal{C}_+ : \frac{\#\{j : C_j \leq -t\}}{\#\{j : C_j \geq t\} \vee 1} \leq q \right\}. \quad (8)$$

With a more conservative knockoff+ filter, the selection set  $\widehat{S}_+ = \{j : C_j \geq \tau_+\}$ , where

$$\tau_+ = \min \left\{ t \in \mathcal{C}_+ : \frac{1 + \#\{j : C_j \leq -t\}}{\#\{j : C_j \geq t\} \vee 1} \leq q \right\}. \quad (9)$$

Here,  $q$  is the target FDR level and  $\mathcal{C}_+ = \{|C_j| : |C_j| > 0\}$ . The theoretical results related to FDR control are provided in Section 5.1.4.

### 2.3 The Algorithm for ZIPG-SK

The Algorithm 1 shows the detailed process of ZIPG-SK in this paper.

---

#### Algorithm 1 The Algorithm for ZIPG-SK.

---

**Input:** Count data matrix  $\mathbf{W}_{n_k \times p}$ ; The labels of  $n_k$  samples  $\mathbf{Y}_k$ ; The covariates  $\mathbf{X}_{n_k \times d}$ ;  $k \in [K]$ ;

**Output:** Synthetic null data  $\widetilde{\mathbf{W}}_k$ ,  $k \in [K]$ ; The filter statistics  $\mathbf{C}$ ; The selection set  $\widehat{S}$  or  $\widehat{S}_+$ ;

- 1: **for** each  $k$  in  $\{1, 2, \dots, K\}$  **do**
  - 2:   Synthetic null generation:  $\widetilde{\mathbf{W}}_k$  based on  $\mathbf{W}_k$ ,  $\mathbf{X}_k$ ;
  - 3:   Calculation of the test statistics:  $\mathbf{Z}_k, \widetilde{\mathbf{Z}}_k$  are calculated by Model-X knockoffs or ClusterDE;
  - 4: **end for**
  - 5: Calculation of the filter statistics: select the appropriate OSFF function to calculate  $\mathbf{C} = f_{OSFF}([\mathbf{Z}_1, \widetilde{\mathbf{Z}}_1], \dots, [\mathbf{Z}_K, \widetilde{\mathbf{Z}}_K])$ .
  - 6: Threshold calculation and feature selection: use the filter statistics  $\mathbf{C}$  and apply the knockoff / knockoff+ filter to obtain  $\widehat{S}$  or  $\widehat{S}_+$ ;
  - 7: **return**  $\widetilde{\mathbf{W}}_k$ ,  $k \in [K]$ ;  $\mathbf{C}$ ;  $\widehat{S}$  or  $\widehat{S}_+$ .
- 

In addition, we can improve the stability and power consumption of the original knockoff algorithm while ensuring false discovery rate control by aggregating multiple knockoffs [25]. Specifically, instead of generating one knockoff copy from each source, we generate  $B$  knockoffs and aggregate them. Typically, the statistics from multiple knockoffs are aggregated using a quantile-based approach to compute the feature statistics. Recently, [21] utilized the aggregation of e-values generated from multiple knockoff realizations to reduce the randomness associated with model-X knockoffs, thereby preserving the power of the original method while mitigating variability. [26] demonstrated that e-values could be readily aggregated by averaging in the context of multiple testing for a single hypothesis. Therefore, this paper also adopts the e-value-based aggregation method to enhance the approach. The specific algorithm (Agg-ZIPG-SK) is presented in Section 5.1.3.

## 3 Simulations

### 3.1 Simulation settings

The simulation experiment primarily includes the generation of the  $k$ -th dataset, as well as the comparison method and strategy. Additionally, we only consider cases where  $\mathbf{Y}_k \in R^{n_k}$  is binary.

The count matrix is set to  $\mathbf{W}_{k, n_k \times p} = [\mathbf{W}_{k,1} \ \mathbf{W}_{k,2}]$ , where  $\mathbf{W}_{k,1}$  are significantly associated with  $\mathbf{Y}_k$  and  $\mathbf{W}_{k,2}$  are irrelevant. The corresponding  $\mathbf{Y}_k$  can be expressed as  $\mathbf{Y}_k = (0_1, \dots, 0_{n_k/2}, 1_{n_k/2+1}, \dots, 1_{n_k})$ . Define the sequencing depth of each sample as  $M^i = \sum_{j=1}^p W_j^i$ . For the  $j$ -th count feature in  $\mathbf{W}_{k,1}$ , we generate different distributions for individuals with different labels  $\mathbf{Y}^k$ . For the  $j$ -th count feature in  $\mathbf{W}_{k,2}$ , we guarantee that all its individuals are drawn from the same distribution. The covariate  $\mathbf{X}_{n_k \times d}$  associated with  $\mathbf{W}^k$  follows a normal distribution, that is,  $\mathbf{X} \sim N_d(\mathbf{0}, \Sigma)$ , where  $\Sigma = (\rho_{i,j})_{d \times d}$ ,  $\rho_{i,j} = 0.1^{|i-j|}$ . Detailed settings for other generic parameters and the generation of simulated count data are provided in Section 5.2.1.

Two knockoff-related construction models, Model-X knockoff and scDesign2 [27], are used for comparison with the proposed method. Model-X knockoff is employed to select high-dimensional control variables. scDesign2 is a transparent simulator that generates count data while capturing variable correlations. It is based on the copula framework and provides multiple options for the marginal distribution (Poisson, NB, and ZINB). In addition, two common strategies, distinct from simultaneous methods, are employed for comparison: Pooling and Intersection. The

former pools  $K$  datasets together and then selects variables for the pooled dataset; the latter selects variables individually for each dataset and takes the intersection of the resulting sets.

### 3.2 Simulation results

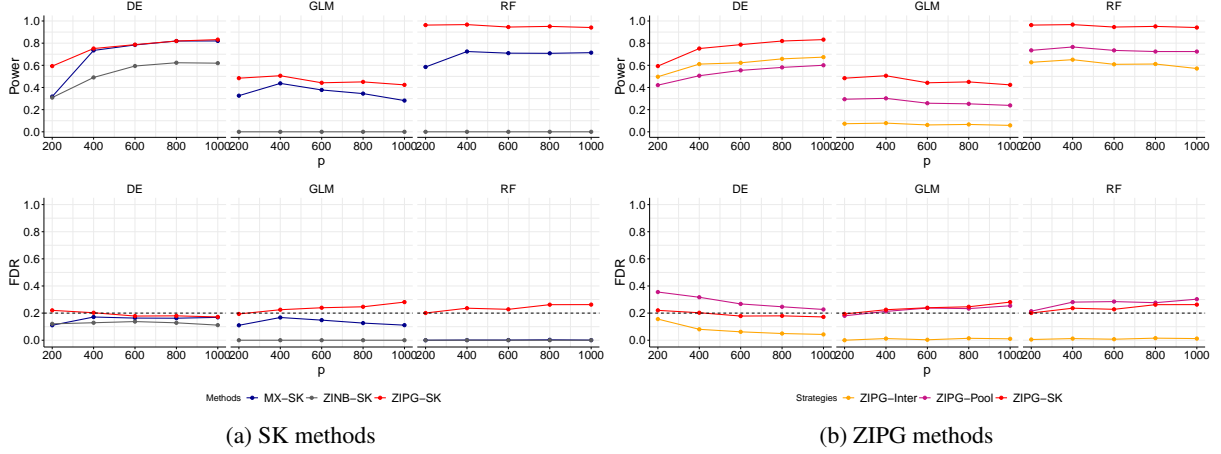


Figure 2: The power and the FDR results of copula-based simulation data. Panel (a) compares different knockoff construction methods within the SK framework, while Panel (b) compares various variable selection strategies based on the ZIPG method. ZIPG, ZINB, and MX represent the data generation methods, while Inter, Pool, and SK represent different strategies of variable set selection. The DE, GLM, and RF represent the methods used for test statistic calculation, respectively. (The methodology descriptions for the subsequent figures are identical to the one provided here.)

For constructing knockoffs, the paper employs Model-X knockoff, scDesign2, and the ZIPG distribution specified by the Gaussian copula (abbreviated as MX, ZINB, and ZIPG, respectively). For three variable selection strategies: Intersection, Pooling, and Simultaneous (abbreviated as Inter, Pool, and SK, respectively). Additionally, this study utilizes clusterDE, glmnet, and random forest to compute test statistics (abbreviated as DE, GLM, and RF, respectively) for comparison purposes. Therefore, the ZIPG-SK method can be further specified as ZIPG-SK-DE, ZIPG-SK-GLM, and ZIPG-SK-RF, each representing the method calculated based on specific statistics.

In a preliminary analysis, we consider the  $K = 2$  first. We set the first 10% count features to be significantly correlated with  $Y$  and the FDR control value for different methods is set to 0.2.

Figure 2 illustrates the outcomes for FDR control and power employing different methods and strategies across 50 experiments. Each dataset has a sample size of 400, with variable dimensions ranging from 200 to 1000. Panels (a) and (b) display results based on three methods (MX-SK, ZINB-SK, and ZIPG-SK) and strategies (ZIPG-Inter, ZIPG-Pool, and ZIPG-SK), with power in the upper plots and FDR in the lower plots. In panel (a), the ZIPG-SK method exhibits consistently strong performance across scenarios compared to MX-SK and ZINB-SK. Its FDR curve under the Simultaneous strategy remains stable across varying variable dimensions, consistently hovering around 0.2. Additionally, power results further underscore the superiority of ZIPG-SK, as it consistently outperforms the other two methods. Panel (b) examines FDR control and power across strategies. Again, the ZIPG-SK presents stable FDR and higher power, whereas the MX-SK and ZINB-SK struggle to control FDR in some instances. For different test statistics, the GLM-based method has lower power (below 0.5) compared to DE and RF methods (over 0.6), likely due to the non-linear relationship between the count data and response variable  $Y$  in the simulations. Further details can be seen in Figure S.1.

This paper also simulates two common issues in multi-source count data: high zero proportions and inconsistent selection sets across sources. Figures S.2 and S.3 display results for zero proportions and variable differences (Diff) across datasets. The ZIPG-SK method demonstrates stable FDR control across varying zero proportions, indicating robust performance. While FDR slightly increases with Diff for three methods, the proposed method consistently maintains optimal FDR control and achieves superior power across scenarios.

The paper compares results from the Aggregating algorithm (Agg-ZIPG-SK), the standard ZIPG-SK method, and a non-covariate version (ZIPG-SK-nonx). Here, Agg-ZIPG-SK is an aggregated form of ZIPG-SK, while ZIPG-SK-nonx

excludes covariate information. Figure 3 shows FDR and power outcomes for all three cases. The ZIPG-SK and ZIPG-SK-nonnx methods produce similar results, likely because the ZIPG-SK model includes sequencing depth, which may have a stronger impact than covariates in data generation. Although power is comparable between Agg-ZIPG-SK and ZIPG-SK in Simultaneous scenarios, Agg-ZIPG-SK achieves better FDR control, underscoring the effectiveness of the e-value-based approach.

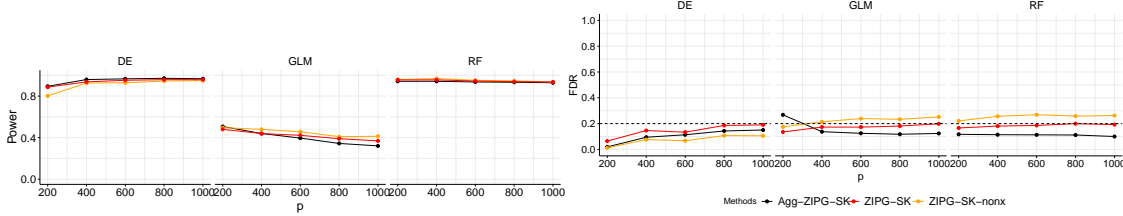


Figure 3: The power and the FDR based on Aggregating algorithm.

This paper also investigates non-copula scenarios and the case with  $K=3$ . These additional results demonstrate similar patterns and trends as previous results. Moreover, this paper provides further discussion on the simulations described above, including the selection of OSFF functions in the algorithm. More detailed information is discussed in the Section 5.2.

## 4 Real Data Analysis

The association between gut microbiota and CRC has been extensively investigated in numerous studies [28]. However, it is improbable that all gut microbes exhibit strong associations with CRC. Significant variations in intestinal microbial composition exist among individuals from different regions. Thus, our objective is to employ ZIPG-SK method to explore the gut microbiota associated with CRC across multiple geographical regions.

To ensure result stability, this study adopts a five-fold cross-validation (CV) approach. In each iteration, four folds of data are for variable selection, and integrated results from the five CV iterations form one CV result. This process is repeated 30 times to obtain comprehensive outcomes. Furthermore, in conjunction with the exploration of different methods and strategies, this paper includes a comparison with two commonly used variable selection methods for gut microbial data: clr-lasso [29] and coda-lasso [30]. Clr-lasso relies on the centered log-ratio transformation (clr), while coda-lasso employs a log-contrast model. These methods serve as benchmarks for evaluating the performance of the proposed approach.

Figure 4 illustrates the number and overlap of selected gut microbes using different methods and strategies. The venn diagram and upset diagram depict these results. Panel (a) of Figure 4 shows the outcomes obtained from the various methods and strategies compared in this paper. It is observed that the Pooling strategy generally selects a larger number of gut microbes, followed by the Simultaneous method, while the Intersection strategy yields the fewest selections, or even zero. Additionally, more gut microbes are chosen using the DE approach compared to the GLM and RF approaches. These results are reasonable since the Pooling strategy combines all the data for variable selection, resulting in a larger dataset. Moreover, if the gut microbiome data from any region are associated with CRC, the pooled data is more likely to be related as well. Furthermore, the DE approach calculates statistics based on tests like the wilcoxon test, which tends to select a higher number of variables compared to GLM and RF. The Intersection and Simultaneous strategies select fewer gut microbes, as evidenced by the presence of only two variables in the intersection set of the upper half of the upset plot. Panel (b) presents the outcomes under the Simultaneous-based strategy. It is evident that although the Simultaneous method generally selects only a few variables, there is significant overlap among the majority of the chosen gut microbes. Therefore, panels (a) and (b) primarily demonstrate the effectiveness of the ZIPG-SK methods.

The ZIPG-SK methods successfully identify six gut microbes at the species level that show associations with CRC in various regions. Among these gut microbes, five of them overlapped, namely *Fusobacterium nucleatum* (*F. nucleatum*), *Gemella morbillorum* (*G. morbillorum*), *Parvimonas micra* (*P. micra*), *Parvimonas unclassified* (*P. unclassified*), and *Peptostreptococcus stomatis* (*P. stomatis*). Among them, *F. nucleatum*, *G. morbillorum*, and *C. morbillorum* were found to be consistent with the results of [7]. [7] also incorporated shotgun metagenomic sequencing data from several geographical populations. However, the feature selection in their study was based on pooling or aggregation, resulting in the selection of more gut microbes than the method used in this paper. The findings for the two gut microbes identified here, *P. stomatis* and *F. nucleatum*, align with those reported by [31]. [31] investigated the regional differences in metagenomic datasets of gut microbes from six countries. Their analysis revealed a shared diversity of bacteria among



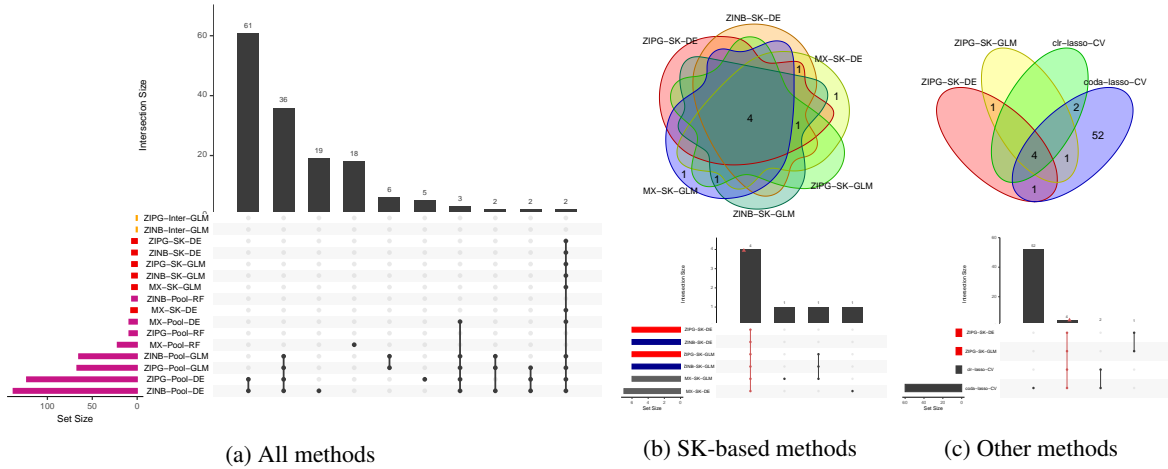


Figure 4: The number and overlap of selected gut microbial variables under different methods and strategies. Panel (a) displays the results obtained using various method strategies explored in this paper. ZIPG, ZINB, and MX represent the data generation methods, while DE, GLM, and RF represent the methods used for test statistic calculation. The letters I, P, and S signify the Intersection, Pooling, and Simultaneous strategies of variable set selection, respectively. Panel (b) presents the results obtained using the Simultaneous strategy. Panel (c) presents a comparison between the final method (ZIPG-SK-DE, ZIPG-SK-GLM) and the two penalty regression methods discussed in this paper.

these countries, particularly at the species level. Additionally, the gut microbe P. unclassified may not have similar results in the existing literature, but it could play a guiding role in further research.

Furthermore, panel (c) in Figure 4 presents a comparison between the ZIPG-SK methods (ZIPG-SK-DE and ZIPG-SK-GLM) and two penalized regression methods, clr-lasso and coda-lasso. ZIPG-SK-DE and ZIPG-SK-GLM are based on the ZIPG model and simultaneous strategies. Clr-lasso and coda-lasso are applied to results obtained from pooling and CV, respectively. Clr-lasso selects 6 gut microorganisms, while coda-lasso selects 60 microorganisms, with an overlap of 4 microorganisms across the four methods. These results are consistent with previous findings and demonstrate improved effectiveness. We also perform a classification diagnosis of CRC based on gut microbial selection results from the four methods (Table S.2). The classification accuracy of the four methods is comparable. Although the method proposed in this paper selects relatively fewer gut microbes, it still demonstrates strong effectiveness in subsequent classification diagnosis, confirming the efficacy of the presented method. Further details are provided in Section 5.3.2.

In summary, the proposed method effectively identifies common gut microbial markers from diverse sources using multi-country gut microbial datasets. Additionally, the above analysis is conducted using the Simultaneous method in the OSFF mode of Direct Diff Dot product, while results based on other OSFF cases are discussed in Section 5.3.4.

### 4.1 Repeatability Analysis: Single-cell dataset of T2D

To further validate the reproducibility of the ZIPG-SK method in multi-source studies, the analysis processes are implemented identically based on single-cell data for T2D. This section focuses on the differentially expressed genes (DEGs) across various cell types in healthy individuals and patients with T2D.

Initially, 2000 highly variable genes are pre-screened using the Seurat package, followed by the application of the ZIPG-SK method to select DEGs from the pre-screened single-cell data from multiple sources. Table S.5 presents the DEGs identified across all six cell types. These DEGs act as markers for distinguishing healthy individuals from patients with T2D. For instance, a correlation has been observed between the methylation of the *INS* gene promoters and the regulation of *INS* gene expression in islets and pancreatic  $\beta$  cells [32]. Additionally, [33] proposed that polymorphisms in the *CLPS* gene could be considered genetic risk factors for T2D.

GO enrichment analysis is conducted on the identified DEGs. Figure S.12 displays enriched bubble maps that highlight the top 10 enriched functional classes in Biological Processes (BP), Cellular Components (CC), and Molecular Functions (MF). For instance, in terms of BP, it elucidates the pivotal role of islet cells in immune regulation, antigen recognition, and stress response. The biological processes involve Interferon signaling pathways, antigen processing and presentation of endogenous peptide antigens/exogenous peptide antigens under the MHC I pathway, and protection against immune

cell-mediated cytotoxicity. Among these processes, the Interferon signaling pathway may serve as a critical regulator of immune and inflammatory responses in islets, thereby influencing the stability and function of islet cells [34]. The latter two processes are also linked to inflammation and immunity [35]. These enriched functions essentially highlight significant distinctions between healthy individuals and those with T2D.

This study compares our method with two others (clr-lasso and coda-lasso). Figure S.11 illustrates the overlapping selected genes using Venn diagrams. The 6 DEGs selected by the ZIPG-SK method are also identified by the other two methods. Additionally, DEGs across multiple cell types are explored, including all six cell types, three cell types ( $\alpha$  cells,  $\beta$  cells, and  $\delta$  cells), and two cell types ( $\alpha$  cells and  $\beta$  cells). Consistently fewer DEGs are identified by ZIPG-SK compared to the other two methods among the three scenarios. Based on the trend in the number of DEGs selected, the method proposed in this paper demonstrates improved capability in handling the heterogeneity of multi-source data, potentially enhancing the selection of common DEGs across multiple sources. Further details are provided in Section 5.4.

## 5 Conclusion

The Zero-Inflated Poisson-Gamma based Simultaneous Knockoff (ZIPG-SK) for Multi-source Count Data is a versatile framework designed for testing null hypotheses concerning conditional associations between candidate count features and outcomes. This paper focuses on the variable selection problem for multi-source count data using the knockoff framework. In this study, we introduce the Gaussian copula and ZIPG distribution to model and synthesize the count data, incorporating covariate information. The calculations of statistics and FDR control are then performed using the general knockoff method to address the variable selection problem in multi-source datasets. Simulation results and real data analysis demonstrate the superior performance of our proposed method compared to the Simultaneous Knockoff method in processing count data.

Furthermore, count data encompasses a wide range of application scenarios beyond the examples discussed in this paper. It includes diverse data types such as gut microbiome data from different regions and common single-cell sequencing data. For instance, [36] investigated brain tumor heterogeneity through multi-sector single-cell RNA sequencing, characterizing and constructing chemokine profiles between different tumor and non-tumor cells.

Our approach opens up numerous possibilities for extension and further exploration. Firstly, although we consider the impact of covariates (clinical factors) in this study, our simulation and actual data analysis reveal that the inclusion of a few clinical factors does not exert a substantial influence on the final results, as illustrated in Figure S.6 of the Section 5.2.5. This observation may be attributed to the limited relevance of the covariates considered in relation to the actual candidate microorganisms. Secondly, although the simulation and data analysis primarily address classification diagnosis problems involving binary response variables, our method can be readily applied to scenarios involving continuous or mixed response variables. Moreover, our current method primarily emphasizes the selection of individual count features. However, count features, such as intestinal microorganisms, often exhibit hierarchical structures, such as at the family or species levels, implying inherent grouping. In future research, it would be valuable to explore group-level or multi-level variable selection methods, such as the Multilayer Knockoff Filter (MKF) [37], to delve deeper into the selection of count feature groups.

## Data and Code Availability

The metagenomic sequencing data analyzed in this study are available in the Sequence Read Archive (SRA) and the European Nucleotide Archive (ENA). The single-cell diabetes dataset is sourced from the European Molecular Biology Laboratory - European Bioinformatics Institute (EMBL-EBI).

## Funding

This work was supported by the National Natural Science Foundation of China [12071119, 12401381], the National Social Science Foundation Project [20BTJ035], and the Postgraduate Scientific Research Innovation Project of Hunan Province [CX20230417].

## References

- [1] Karrie KK Ko, Kern Rei Chng, and Niranjan Nagarajan. Metagenomics-enabled microbial surveillance. *Nature Microbiology*, 7(4):486–496, 2022.
- [2] Nicholas Bradley Larson, Ann L Oberg, Alex A Adjei, and Ligu Wang. A clinician’s guide to bioinformatics for next-generation sequencing. *Journal of Thoracic Oncology*, 18(2):143–157, 2023.
- [3] Emmanuel Candès, Yingying Fan, Lucas Janson, and Jinchi Lv. Panning for gold: ‘model-x’ knockoffs for high dimensional controlled variable selection. *Journal of the Royal Statistical Society Series B: Statistical Methodology*, 80(3):551–577, 2018.
- [4] Hangjin Jiang and Xiaodan Fan. A consistent variable screening procedure with family-wise error control. *Journal of Statistical Computation and Simulation*, 90(7):1267–1285, 2020.
- [5] Tao Wang and Hongyu Zhao. Constructing predictive microbial signatures at multiple taxonomic levels. *Journal of the American Statistical Association*, 112(519):1022–1031, 2017.
- [6] Yukie Kashima, Yoshitaka Sakamoto, Keiya Kaneko, Masahide Seki, Yutaka Suzuki, and Ayako Suzuki. Single-cell sequencing techniques from individual to multiomics analyses. *Experimental & Molecular Medicine*, 52(9):1419–1427, 2020.
- [7] Ning-Ning Liu, Na Jiao, Jing-Cong Tan, Ziliang Wang, Dingfeng Wu, An-Jun Wang, Jie Chen, Liwen Tao, Chenfen Zhou, Wenjie Fang, et al. Multi-kingdom microbiota analyses identify bacterial–fungal interactions and biomarkers of colorectal cancer across cohorts. *Nature Microbiology*, 7(2):238–250, 2022.
- [8] Raphael Petegrosso, Zhuliu Li, and Rui Kuang. Machine learning and statistical methods for clustering single-cell rna-sequencing data. *Briefings in bioinformatics*, 21(4):1209–1223, 2020.
- [9] Lukas Heumos, Anna C Schaar, Christopher Lance, Anastasia Litinetskaya, Felix Drost, Luke Zappia, Malte D Lücken, Daniel C Strobl, Juan Henao, Fabiola Curion, et al. Best practices for single-cell analysis across modalities. *Nature Reviews Genetics*, pages 1–23, 2023.
- [10] Wei Lin, Pixu Shi, Rui Feng, and Hongzhe Li. Variable selection in regression with compositional covariates. *Biometrika*, 101(4):785–797, 2014.
- [11] Dongyuan Song, Kexin Li, Xinzhou Ge, and Jingyi Jessica Li. Clusterde: a post-clustering differential expression (de) method robust to false-positive inflation caused by double dipping. *bioRxiv*, pages 2023–07, 2023.
- [12] Chih-Wen Chen, Yi-Hong Tsai, Fang-Rong Chang, and Wei-Chao Lin. Ensemble feature selection in medical datasets: Combining filter, wrapper, and embedded feature selection results. *Expert Systems*, 37(5):e12553, 2020.
- [13] Tristan Mary-Huard, Jean-Jacques Daudin, Michela Baccini, Annibale Biggeri, and Avner Bar-Hen. Biases induced by pooling samples in microarray experiments. *Bioinformatics*, 23(13):i313–i318, 2007.
- [14] Shinyuu Lee and Yuru Zhu. Confounder selection via support intersection. *arXiv preprint arXiv:1912.11652*, 2019.
- [15] Rina Foygel Barber and Emmanuel J. Candès. Controlling the false discovery rate via knockoffs. *The Annals of Statistics*, 43(5):2055 – 2085, 2015.
- [16] Xin Bai, Jie Ren, Yingying Fan, and Fengzhu Sun. Kimi: Knockoff inference for motif identification from molecular sequences with controlled false discovery rate. *Bioinformatics*, 37(6):759–766, 2021.
- [17] Gianna Serafina Monti and Peter Filzmoser. A robust knockoff filter for sparse regression analysis of microbiome compositional data. *Computational Statistics*, pages 1–18, 2022.
- [18] Divan Aristo Burger, Robert Schall, Johannes Theodorus Ferreira, and Ding-Geng Chen. A robust bayesian mixed effects approach for zero inflated and highly skewed longitudinal count data emanating from the zero inflated discrete weibull distribution. *Statistics in Medicine*, 39(9):1275–1291, 2020.
- [19] Ran Dai and Cheng Zheng. False discovery rate-controlled multiple testing for union null hypotheses: a knockoff-based approach. *Biometrics*, 2023.
- [20] Roulan Jiang, Xiang Zhan, and Tianying Wang. A flexible zero-inflated poisson-gamma model with application to microbiome sequence count data. *Journal of the American Statistical Association*, 118(542):792–804, 2023.
- [21] Zhimei Ren and Rina Foygel Barber. Derandomised knockoffs: leveraging e-values for false discovery rate control. *Journal of the Royal Statistical Society Series B: Statistical Methodology*, 86(1):122–154, 2024.
- [22] Åsa Segerstolpe, Athanasia Palasantza, Pernilla Eliasson, Eva-Marie Andersson, Anne-Christine Andréasson, Xiaoyan Sun, Simone Picelli, Alan Sabirsh, Maryam Clausen, Magnus K Bjursell, et al. Single-cell transcriptome profiling of human pancreatic islets in health and type 2 diabetes. *Cell metabolism*, 24(4):593–607, 2016.

- [23] Chun-Shu Chen and Chung-Wei Shen. Distribution-free model selection for longitudinal zero-inflated count data with missing responses and covariates. *Statistics in Medicine*, 41(16):3180–3198, 2022.
- [24] Fatemeh Sarvi, Abbas Moghimbeigi, and Hossein Mahjub. Gee-based zero-inflated generalized poisson model for clustered over or under-dispersed count data. *Journal of Statistical Computation and Simulation*, 89(14):2711–2732, 2019.
- [25] Tuan-Binh Nguyen, Jérôme-Alexis Chevalier, Bertrand Thirion, and Sylvain Arlot. Aggregation of multiple knockoffs. In *International Conference on Machine Learning*, pages 7283–7293. PMLR, 2020.
- [26] Vladimir Vovk and Ruodu Wang. E-values: Calibration, combination and applications. *The Annals of Statistics*, 49(3):1736–1754, 2021.
- [27] Tianyi Sun, Dongyuan Song, Wei Vivian Li, and Jingyi Jessica Li. scdesign2: a transparent simulator that generates high-fidelity single-cell gene expression count data with gene correlations captured. *Genome biology*, 22(1):163, 2021.
- [28] Chi Chun Wong and Jun Yu. Gut microbiota in colorectal cancer development and therapy. *Nature Reviews Clinical Oncology*, 20(7):429–452, 2023.
- [29] Antoni Susin, Yiwen Wang, Kim-Anh Lê Cao, and M Luz Calle. Variable selection in microbiome compositional data analysis. *NAR Genomics and Bioinformatics*, 2(2):lqaa029, 2020.
- [30] Jiarui Lu, Pixu Shi, and Hongzhe Li. Generalized linear models with linear constraints for microbiome compositional data. *Biometrics*, 75(1):235–244, 2019.
- [31] Han Shuwen, Wu Yinhang, Zhao Xingming, Zhuang Jing, Liu Jinxin, Wu Wei, and Ding Kefeng. Using whole-genome sequencing (wgs) to plot colorectal cancer-related gut microbiota in a population with varied geography. *Gut Pathogens*, 14(1):50, 2022.
- [32] Ollin Celeste Martínez-Ramírez, Azucena Salazar-Piña, Ximena Cerón-Ramírez, Julieta Rubio-Lightbourn, Fernando Torres-Romero, Leonora Casas-Avila, and Clementina Castro-Hernández. Effect of inulin intervention on metabolic control and methylation of ins and irs1 genes in patients with type 2 diabetes mellitus. *Nutrients*, 14(23):5195, 2022.
- [33] Zsuzsanna Jaczó, Eszter Pál, Réka Dénes, Anikó Somogyi, Mária Sasvári-Székely, András Guttman, and Zsolt Rónai. Rapid analysis of colipase gene variants by multicapillary electrophoresis. *Electrophoresis*, 36(11-12):1237–1243, 2015.
- [34] P Kent Langston, Yizhi Sun, Birgitta A Ryback, Amber L Mueller, Bruce M Spiegelman, Christophe Benoist, and Diane Mathis. Regulatory t cells shield muscle mitochondria from interferon- $\gamma$ -mediated damage to promote the beneficial effects of exercise. *Science immunology*, 8(89):eadi5377, 2023.
- [35] Lina Wang, Xiangqian Li, Shushu Yang, Xiaoling Chen, Jie Li, Shufeng Wang, Mengjun Zhang, Zhengni Zheng, Jie Zhou, Li Wang, et al. Proteomic identification of mhc class i-associated peptidome derived from non-obese diabetic mouse thymus and pancreas. *Journal of proteomics*, 270:104746, 2023.
- [36] Kai Yu, Yuqiong Hu, Fan Wu, Qiufang Guo, Zenghui Qian, Waner Hu, Jing Chen, Kuanyu Wang, Xiaoying Fan, Xinglong Wu, et al. Surveying brain tumor heterogeneity by single-cell rna-sequencing of multi-sector biopsies. *National science review*, 7(8):1306–1318, 2020.
- [37] Eugene Katsevich and Chiara Sabatti. Multilayer knockoff filter: Controlled variable selection at multiple resolutions. *The annals of applied statistics*, 13(1):1, 2019.
- [38] Achim Zeileis, Christian Kleiber, and Simon Jackman. Regression models for count data in r. *Journal of statistical software*, 27(8):1–25, 2008.
- [39] Xinzhou Ge, Yiling Elaine Chen, Dongyuan Song, MeiLu McDermott, Kyla Woyshner, Antigoni Manousopoulou, Ning Wang, Wei Li, Leo D Wang, and Jingyi Jessica Li. Clipper: p-value-free fdr control on high-throughput data from two conditions. *Genome biology*, 22(1):1–29, 2021.
- [40] Tzu-Wei Yang, Wei-Hsiang Lee, Siang-Jyun Tu, Wei-Chih Huang, Hui-Mei Chen, Ting-Hsuan Sun, Ming-Chang Tsai, Chi-Chih Wang, Hsuan-Yi Chen, Chi-Chou Huang, et al. Enterotype-based analysis of gut microbiota along the conventional adenoma-carcinoma colorectal cancer pathway. *Scientific reports*, 9(1):1–13, 2019.
- [41] Jun Yu, Qiang Feng, Sunny Hei Wong, Dongya Zhang, Qiao yi Liang, Youwen Qin, Longqing Tang, Hui Zhao, Jan Stenvang, Yanli Li, et al. Metagenomic analysis of faecal microbiome as a tool towards targeted non-invasive biomarkers for colorectal cancer. *Gut*, 66(1):70–78, 2017.
- [42] Georg Zeller, Julien Tap, Anita Y Voigt, Shinichi Sunagawa, Jens Roat Kultima, Paul I Costea, Aurélien Amiot, Jürgen Böhm, Francesco Brunetti, Nina Habermann, et al. Potential of fecal microbiota for early-stage detection of colorectal cancer. *Molecular systems biology*, 10(11):766, 2014.

- [43] Jakob Wirbel, Paul Theodor Pyl, Ece Kartal, Konrad Zych, Alireza Kashani, Alessio Milanese, Jonas S Fleck, Anita Y Voigt, Albert Palleja, Ruby Ponnudurai, et al. Meta-analysis of fecal metagenomes reveals global microbial signatures that are specific for colorectal cancer. *Nature medicine*, 25(4):679–689, 2019.
- [44] Shinichi Yachida, Sayaka Mizutani, Hirotugu Shiroma, Satoshi Shiba, Takeshi Nakajima, Taku Sakamoto, Hikaru Watanabe, Keigo Masuda, Yuichiro Nishimoto, Masaru Kubo, et al. Metagenomic and metabolomic analyses reveal distinct stage-specific phenotypes of the gut microbiota in colorectal cancer. *Nature medicine*, 25(6):968–976, 2019.
- [45] Emily Vogtmann, Xing Hua, Georg Zeller, Shinichi Sunagawa, Anita Y Voigt, Rajna Hercog, James J Goedert, Jianxin Shi, Peer Bork, and Rashmi Sinha. Colorectal cancer and the human gut microbiome: reproducibility with whole-genome shotgun sequencing. *PloS one*, 11(5):e0155362, 2016.
- [46] Amir Mohammad Malvandi, Cristian Loretelli, Moufida Ben Nasr, Gian Vincenzo Zuccotti, and Paolo Fiorina. Sitagliptin favorably modulates immune-relevant pathways in human beta cells. *Pharmacological research*, 148:104405, 2019.
- [47] Jeannig Berrou, Sophie Fougeray, Marion Venot, Victor Chardiny, Jean-François Gautier, Nicolas Dulphy, Antoine Toubert, and Marie-Noëlle Peraldi. Natural killer cell function, an important target for infection and tumor protection, is impaired in type 2 diabetes. *PloS one*, 8(4):e62418, 2013.
- [48] Geng Zhang, Peijun He, Hanson Tan, Anuradha Budhu, Jochen Gaedcke, B Michael Ghadimi, Thomas Ried, Harris G Yfantis, Dong H Lee, Anirban Maitra, et al. Integration of metabolomics and transcriptomics revealed a fatty acid network exerting growth inhibitory effects in human pancreatic cancer. *Clinical cancer research*, 19(18):4983–4993, 2013.
- [49] Maria Karsai, Richard A Zuellig, Roger Lehmann, Federica Cuzzo, Daniela Nasteska, Edlira Luca, Constanze Hantel, David J Hodson, Giatgen A Spinas, Guy A Rutter, et al. Lack of znt8 protects pancreatic islets from hypoxia-and cytokine-induced cell death. *Journal of Endocrinology*, 253(1):1–11, 2022.
- [50] Inka Lindner, Ulf Helwig, Diana Rubin, Yun Li, Eva Fisher, Heiner Boeing, Matthias Möhlig, Joachim Spranger, Andreas Pfeiffer, Jochen Hampe, et al. Putative association between a new polymorphism in exon 3 (arg109cys) of the pancreatic colipase gene and type 2 diabetes mellitus in two independent caucasian study populations. *Molecular nutrition & food research*, 49(10):972–976, 2005.
- [51] Muhmmad Omar-Hmeadi and Olof Idevall-Hagren. Insulin granule biogenesis and exocytosis. *Cellular and Molecular Life Sciences*, 78:1957–1970, 2021.
- [52] Francesco Piarulli, Cristina Banfi, Eugenio Ragazzi, Erica Gianazza, Marco Munno, Massimo Carollo, Pietro Traldi, Annunziata Lapolla, and Giovanni Sartore. Multiplexed mrm-based proteomics for identification of circulating proteins as biomarkers of cardiovascular damage progression associated with diabetes mellitus. *Cardiovascular Diabetology*, 23(1):36, 2024.
- [53] Mohammed F Gholam, Lauren P Liu, Louis A Searcy, Nancy D Denslow, and Abdel A Alli. Dapagliflozin treatment augments bioactive phosphatidylethanolamine concentrations in kidney cortex membrane fractions of hypertensive diabetic db/db mice and alters the density of lipid rafts in mouse proximal tubule cells. *International Journal of Molecular Sciences*, 24(2):1408, 2023.
- [54] Eunhee Choi and Xiao-Chen Bai. The activation mechanism of the insulin receptor: a structural perspective. *Annual review of biochemistry*, 92(1):247–272, 2023.
- [55] Zhongqin Chen, Xiaojie Su, Wenhong Cao, Mingtang Tan, Guoping Zhu, Jialong Gao, and Longjian Zhou. The discovery and characterization of a potent dpp-iv inhibitory peptide from oysters for the treatment of type 2 diabetes based on computational and experimental studies. *Marine Drugs*, 22(8):361, 2024.
- [56] Abdul-Hamid Emwas, Mawadda Alghrably, Manel Dhahri, Abeer Sharfalddin, Rawiah Alsiary, Mariusz Jaremko, Gavino Faa, Marcello Campagna, Terenzio Congiu, Monica Piras, et al. Living with the enemy: From protein-misfolding pathologies we know, to those we want to know. *Ageing Research Reviews*, 70:101391, 2021.

## Supplement

This supplement provides additional details and related results for Zero Inflated Poisson-Gamma based Simultaneous knockoff (ZIPG-SK).

In Section 5.1, we elaborate on the statistical framework involved in ZIPG-SK, including the EM Algorithm for the ZIPG model, the construction of simultaneous knockoffs, and the aggregation algorithm for ZIPG-SK. Additionally, we discuss theoretical results supporting our methodology. Section 5.2 presents supplementary simulation results

that expand upon those provided in the main text. These experiments further validate the robustness of the proposed approach. In Section 5.3, we focus on the specifics and characteristics of the real-world dataset, particularly the multi-source colorectal cancer (CRC) data. This section includes a comparative analysis of variable selection outcomes across different methodologies, with an emphasis on CRC classification diagnosis and results derived from other OSFF scenarios. Section 5.4 describes a comparable replication study conducted using multi-source data related to type 2 diabetes (T2D).

In summary, this supplement provides additional insights and findings on the ZIPG-SK method, enhancing our understanding of the impacts of various approaches in multi-source count data analysis.

## 5.1 Details of the method

### 5.1.1 Parameter estimation

First, the parameter of the  $j$ -th count feature in the ZIPG model is  $\Omega = (\beta_0, \beta^T, \beta_0^*, \beta^{*T}, \gamma)^T$ , where  $\gamma = \log\{\pi/(1-\pi)\}$  is the logit transformation of zero-inflated parameter  $\pi$  in ZIPG model. These parameters are estimated by employing the Expectation Maximization Algorithm for the  $p$  ZIPG distributions. Based on the estimated parameters  $\hat{\Omega}$ , the corresponding CDFs are denoted as  $\hat{F}_1, \dots, \hat{F}_p$ .

Second, to estimate  $\mathbf{R}$ , each  $W_j^i$  is first transformed as  $U_j^i = V_j^i \cdot \hat{F}_j(W_j^i) + (1 - V_j^i) \cdot \hat{F}_j(W_j^i + 1)$ , where  $V_j^i \stackrel{\text{i.i.d.}}{\sim} \text{Uniform}[0, 1]$ , so that  $U_j^i \sim \text{Uniform}[0, 1]$ . This procedure is referred to as the "distribution transform" to convert a discrete random variable  $W_j^i$  to a continuous Uniform[0,1] random variable. Then, the  $\mathbf{R}$  is estimated as the sample correlation matrix of

$$(\Phi^{-1}(U_1^1), \dots, \Phi^{-1}(U_p^1))^T, \dots, (\Phi^{-1}(U_1^n), \dots, \Phi^{-1}(U_p^n))^T$$

and denoted as  $\hat{\mathbf{R}}$ .

In summary, the fitted null model parameters include  $\hat{\Omega}$  and  $\hat{\mathbf{R}}$ .

The details of the **Expectation Maximization Algorithm for the ZIPG model** are as follows:

The parameter estimation of the ZIPG model primarily follows that described in [20], which is a well-regarded approach in the field. The main difference lies in this study's consideration of all covariates in both link functions and its exclusion of multiple measurements from the same sample. For ease of presenting, we omit the subscript  $j$  and denote the parameter set associated with count feature  $j$  as  $\Omega = (\beta_0, \beta^T, \beta_0^*, \beta^{*T}, \gamma)^T$ , where  $\gamma = \log\{\pi/(1-\pi)\}$ .

Under the null model, we assume that  $W_j^i$ , variable  $j$ 's count value in individual  $i$ , independently follows the hierarchical Zero-Inflated Poisson-Gamma  $ZIPG(\lambda, \theta, \pi_j)$  distribution with the probability mass function:

$$P_{ZIPG}(W; \lambda, \theta, \pi_j) = \pi_j \delta_0(W) + (1 - \pi_j) P_{PG}(W; \lambda, \theta),$$

$$P_{PG}(W = w | \lambda, \theta) = \frac{\Gamma(w + \theta^{-1})}{\Gamma(w + 1)\Gamma(\theta^{-1})} \frac{(\lambda\theta)^w}{(1 + \lambda\theta)^{\theta^{-1} + w}},$$

where  $\delta_0$  is the Dirac function and  $\Gamma(\cdot)$  is the Gamma function. The above PG distribution is basically equivalent to the negative binomial distribution  $NB(\mu, \alpha)$  when  $\mu = \lambda$ ,  $\alpha = \theta$  is satisfied, where  $\mu$  and  $\alpha$  are the mean parameter and (over-)dispersion parameter.

Given covariates  $X$ , observed count data  $W$  and sequencing depth  $M$ , we write the log-likelihood of  $\Omega$  as follows:

$$L(\Omega | \mathbf{W}) = \sum_{i=1}^n [I(W^i = 0) \log\{\exp(\gamma) + P_{PG}(W^i | \Omega)\} \\ + I(W^i > 0) \log\{P_{PG}(W^i | \Omega)\} \\ - \log\{\exp(\gamma) + 1\}],$$

where  $\lambda^i$  and  $\theta^i$  are functions of  $\Omega$  and the log-likelihood is nonconcave in  $\Omega$ . However, directly maximizing  $L(\Omega | \mathbf{W})$  can cause difficulties in distinguishing zeros from the Poisson-Gamma part and the other zero-inflation part of the ZIPG model, leading to an unreasonably low estimate of  $\gamma$ .

Here, the Expectation Maximization (EM) algorithm is used for a reliable estimator of  $\Omega$ . Let  $z^i$  be the latent variable, where  $z^i = 1$  indicates  $W^i$  is generated from zero-inflated part with probability  $\pi = \exp(\gamma)/(\exp(\gamma) + 1)$ , and  $z^i = 0$

indicates  $W^i$  is generated from the Poisson-Gamma distribution with probability  $1 - \pi$ . The log-likelihood with complete data  $\{W^i, M^i, X^i, z^i\}$  for  $i = 1, \dots, n$  is written as

$$L(\Omega | \mathbf{W}, \mathbf{z}) = \sum_i [z^i \log(\pi) + (1 - z^i) \log \{(1 - \pi) P_{\text{PG}}(W^i | \Omega)\}]. \quad (10)$$

Firstly, initialize  $\Omega^{(0)}$  using the results from the `zeroinfl` function in the `pscl` package [38] with  $\beta^* = \mathbf{0}$ .  $\pi^{(0)}$  is adjusted to the proportion to observed zeros of  $\mathbf{W}$  to avoid the local maximum at the start point. Then, repeat the E-step and M-step until convergence or the maximum number of iterations  $t_{\max}$  is reached.

For the  $t$ -th iteration, in M-step, update  $\Omega$  by maximizing Equation 10 given the latent variable  $z^{(t-1)}$ :

$$\Omega^{(t)} = \arg \max L(\Omega | \mathbf{W}, \mathbf{z}^{(t-1)}). \quad (11)$$

Use the BFGS method in the R function `'optim'`, and apply the gradient of Equation 10 to improve computational efficiency.

In E-step, update the latent variables  $z_i$  using their conditional expectations given  $\Omega^{(t)}$  estimated from the M-step:

$$\begin{aligned} z_i^{(t)} &= E\{z_i | W^i, \Omega^{(t)}\} \\ &= \frac{I(W^i = 0)\pi^{(t)}}{I(W^i = 0)\pi^{(t)} + P_{\text{PG}}(W^i | \Omega^{(t)})(1 - \pi^{(t)})}. \end{aligned} \quad (12)$$

By substituting the latent variables  $z_i^{(t)} = z(W^i, \Omega^{(t)})$  into Equation 10, the expectation of the log-likelihood for a single observation can be expressed as a new function,

$$\begin{aligned} Q_i(\Omega | \Omega^{(t)}) &= E\{L(\Omega | W^i, z^i) | W^i, \Omega^{(t)}\} \\ &= z(W^i, \Omega^{(t)}) \log \pi + \{1 - z(W^i, \Omega^{(t)})\} \log \{(1 - \pi) P_{\text{PG}}(W^i | \Omega)\}, \end{aligned} \quad (13)$$

then  $Q(\Omega | \Omega^{(t)}) = \sum_i Q_i(\Omega | \Omega^{(t)})$  is the quantity maximized in M-step equivalently.

According to [20], based on the suggested initialization, namely the MLE assuming  $\beta^* = 0$  with adjusted  $\pi^{(0)}$ , numerical studies suggest that the estimators are nearly unbiased. The detailed procedure of the EM algorithm is provided in Algorithm 2.

---

#### Algorithm 2 ZIPG EM Algorithm

---

**Input:**  $W, M, X$ , the maximum iterations  $t_{\max}$ , a tolerance  $\epsilon_{\text{tol}}$ .

**Output:**  $\Omega^{(t)}$ .

- 1: Initialize  $\Omega^{(0)}$  by adjusted `pscl` estimation regardless of  $X$ , set  $t = 0$ .
  - 2: Initialize  $\mathbf{z}^{(0)}$  with  $\Omega^{(0)}$  based on Equation 12.
  - 3: Calculate  $L^{(0)} = L(\Omega^{(0)} | \mathbf{W}, \mathbf{z}^{(0)})$  as Equation 10.
  - 4: **while**  $t < t_{\max}$  and  $|L^{(t)} - L^{(0)}|/|L^{(0)}| < \epsilon_{\text{tol}}$  **do**
  - 5:   Given  $\mathbf{z}^{(t-1)}$ , estimate  $\Omega^{(t)}$  by Equation 11 (M-step)
  - 6:   Get the maximized  $L^{(t)} = L(\Omega^{(t)} | \mathbf{W}, \mathbf{z}^{(t-1)})$  as in Equation 10.
  - 7:   Given  $\Omega^{(t)}$ , update  $\mathbf{z}^{(t)}$  by Equation 12 (E-step)
  - 8:    $t = t + 1$ .
  - 9: **end while**
  - 10: **return**  $\Omega^{(t)}$ .
- 

### 5.1.2 Simultaneous knockoff

#### 1. The test statistics

For the individual experiment  $k \in [K]$ , the test statistics  $[\mathbf{Z}_k, \tilde{\mathbf{Z}}_k] \in \mathbb{R}^{2p}$  can be constructed in two ways based on  $W_k, \tilde{W}_k$ : the one is based on Model-X knockoffs, and the other is based on clustering and differential expression (DE) tests.

For the Model-X knockoffs, very general conditional models (such as `glmnet` or random forest) can be used. For example,

- Absolute coefficient (glmnet): We can use  $|\hat{\beta}_j(\lambda)|$  from the penalized generalized linear regression of  $Y$  on  $[\mathbf{W}, \tilde{\mathbf{W}}]$  with either a specific  $\lambda$  value or a  $\hat{\lambda}$  estimated from cross-validation.
- Variable importance factor: We can use the variable importance factors from the random forest fitting of  $Y$  on  $[\mathbf{W}, \tilde{\mathbf{W}}]$  with either fixed tuning parameters or tuning parameters selected from cross-validation.

For the clustering and differential expression (DE) tests, this approach only works when  $y$  is discrete. Specific steps are as follows:

- Clustering: The labels  $Y^1, \dots, Y^n$  of the target data  $\mathbf{W}$  is known. After applying the clustering procedure, we obtain the cluster labels  $\tilde{Y}^1, \dots, \tilde{Y}^n$  from the synthetic null data  $\tilde{\mathbf{W}}$ , respectively, where  $Y^i, \tilde{Y}^i \in \{0, 1\}$ ,  $i = 1, \dots, n$ . Again, there exists no one-to-one correspondence between  $Y^1, \dots, Y^n$  and  $\tilde{Y}^1, \dots, \tilde{Y}^n$ . Any clustering algorithm can be used, such as the common umap+kmeans combination, the Seurat algorithm, and so on.
- DE analysis: Given a DE test, on the target data or synthetic null data, it computes a p-value  $P_j$  for each variable  $j$  for testing the null hypothesis:

$$\text{The target data : } H_{0j} : \mu_{0j} = \mu_{1j},$$

$$\text{The synthetic null data : } \tilde{H}_{0j} : \tilde{\mu}_{0j} = \tilde{\mu}_{1j},$$

where  $\mu_{0j} = \mathbb{E}[W_j^i | Y^i = 0]$ ,  $\mu_{1j} = \mathbb{E}[W_j^i | Y^i = 1]$  and  $\tilde{\mu}_{0j} = \mathbb{E}[\tilde{W}_j^i | \tilde{Y}^i = 0]$ ,  $\tilde{\mu}_{1j} = \mathbb{E}[\tilde{W}_j^i | \tilde{Y}^i = 1]$ . Then the target DE score of variable  $j$  is defined as:

$$S_j := -\log_{10} P_j, \quad \tilde{S}_j := -\log_{10} \tilde{P}_j$$

Common DE tests can be used, such as Wilcoxon rank-sum test, t-test, Kolmogorov-Smirnov test (KS test), and so on.

## 2. The filter statistics

For the individual experiment  $k \in [K]$ , the filter statistics  $\mathbf{C}_k \in \mathbb{R}^p$  can be constructed by anti-symmetric functions based on  $[\mathbf{Z}_k, \tilde{\mathbf{Z}}_k]$ :

- The filter statistics for model-x knockoff are typically constructed based on antisymmetric functions. For example, the difference function and the signed max function,

$$f_{as}([\mathbf{Z}, \tilde{\mathbf{Z}}]) = \mathbf{C} \in \mathbb{R}^p, \text{ where } C_j = Z_j - \tilde{Z}_j,$$

$$f_{as}([\mathbf{Z}, \tilde{\mathbf{Z}}]) = \mathbf{C} \in \mathbb{R}^p, \text{ where } C_j = (Z_j \vee \tilde{Z}_j) \cdot (-1)^{1\{Z_j < \tilde{Z}_j\}}.$$

- The contrast score (filter statistics): To ensure a valid FDR control, Clipper [39] requires each variable to have a contrast score such that the true non-DE variable have contrast scores symmetric about zero. Variable  $j$ 's contrast score  $C_j$  is defined as

$$C_j := S_j - \tilde{S}_j.$$

For the calculation of the filter statistics  $\mathbf{C}$  of  $K$  experiments, we refer to the Simultaneous knockoff framework's One swap flip sign function (OSFF) [19] for construction:

$$\mathbf{C} = f_{OSFF}([\mathbf{Z}_1, \tilde{\mathbf{Z}}_1], \dots, [\mathbf{Z}_K, \tilde{\mathbf{Z}}_K]).$$

For example, Commonly used OSFF are

$$\text{Direct Diff Dot product : } \mathbf{C} = \odot_{k=1}^K (\mathbf{Z}_k - \tilde{\mathbf{Z}}_k),$$

$$\text{Direct Diff Sum : } \mathbf{C} = \sum_{k=1}^K (\mathbf{Z}_k - \tilde{\mathbf{Z}}_k),$$

$$\text{Direct Diff Max : } \mathbf{C} = \max_{k=1}^K (\mathbf{Z}_k - \tilde{\mathbf{Z}}_k),$$

where  $\odot$  denotes the Hadamard product.



**Algorithm 3** The Algorithm of Aggregating multiple for ZIPG-SK (Agg-ZIPG-SK).

---

**Input:** Count data matrix  $\mathbf{W}_{n_k \times p}$ ; The labels of  $n_k$  samples  $\mathbf{Y}_k$ ; The covariates  $\mathbf{X}_{n_k \times d}$ ;  $k \in [K]$ ;  
**Output:** Synthetic null data  $\tilde{\mathbf{W}}_k$ ,  $k \in [K]$ ; The Aggregating statistics  $\mathbf{E}$ ; The selection set  $\hat{S}$  or  $\hat{S}_+$ ;

- 1: **for** each  $b$  in  $\{1, 2, \dots, B\}$  **do**
- 2:   **for** each  $k$  in  $\{1, 2, \dots, K\}$  **do**
- 3:     Synthetic null generation:  $\tilde{\mathbf{W}}_k^b$  based on  $\mathbf{W}_k$ ,  $\mathbf{X}_k$ ;
- 4:     Calculation of the test statistics:  $\mathbf{Z}_k^b, \tilde{\mathbf{Z}}_k^b$  are calculated by Model-X knockoffs or ClusterDE;
- 5:   **end for**
- 6: **end for**
- 7: Aggregation operation (E-value-based approach):  
     AGG test statistics :  
      $\{\mathbf{E}_k^Z, \mathbf{E}_k^{\tilde{Z}}\} = \text{AGG}(\{\mathbf{Z}_k^b, \tilde{\mathbf{Z}}_k^b\}_{b=1}^B)$ ,  
      $\mathbf{C} = f_{OSFF}([\mathbf{E}_1^Z, \tilde{\mathbf{E}}_1^Z], \dots, [\mathbf{E}_K^Z, \tilde{\mathbf{E}}_K^Z])$ , or  
      $= \text{fisher}(p_{[\mathbf{E}_1^Z, \tilde{\mathbf{E}}_1^Z]}, \dots, p_{[\mathbf{E}_K^Z, \tilde{\mathbf{E}}_K^Z]})$ .  
     AGG filter statistics :  
      $\mathbf{C}^b = f_{OSFF}([\mathbf{Z}_1^b, \tilde{\mathbf{Z}}_1^b], \dots, [\mathbf{Z}_K^b, \tilde{\mathbf{Z}}_K^b])$ ,  
      $\mathbf{E}^C = \text{AGG}(\{\mathbf{C}^b\}_{b=1}^B)$ .
- 8: Threshold calculation and feature selection: use the Aggregating statistics  $\mathbf{C}$  or  $\mathbf{E}^C$  to obtain  $\hat{S}$  or  $\hat{S}_+$ ;
- 9: **return**  $\{\tilde{\mathbf{W}}_k\}_{k=1}^K$ ;  $\mathbf{C}$  or  $\mathbf{E}^C$ ;  $\hat{S}$  or  $\hat{S}_+$ .

---

**5.1.3 Algorithm of aggregating multiple for ZIPG-SK.**

Algorithm 3 demonstrates the aggregation operation based on e-values, primarily divided in two parts: the aggregation during the calculation of test statistics and filter statistics. The paper presents the results of FDR control and power using an aggregation approach, with more detailed results available in the Section 5.3.

**5.1.4 Theoretical results****1. Theoretical Results for the Single-Source Case**

A count feature  $W_j$  is said to be ‘null’ if and only if  $Y$  is independent of  $W_j$  conditionally on the other features  $W_{-j} = \{W_1, \dots, W_p\} \setminus \{W_j\}$ . The subset of null feature is denoted by  $\mathcal{H}_0 \subset \{1, \dots, p\}$  and we call a feature  $W_j$  ‘non-null’ or relevant if  $j \notin \mathcal{H}_0$ .

The knockoff construction ( $\tilde{W}_j$ ) is based on sampling the  $W_j$  conditional on all the other count feature (excluding the response), where by ‘sampling’ we explicitly mean drawing a new sample from the conditional distribution of using a random number generator. In this paper, the construction of the knockoff procedure is primarily achieved by sampling from ZIPG specified by the Gaussian copula. It is easy to have

$$\tilde{W}_j \mid (W_{-j}, Y) \stackrel{d}{=} W_j \mid W_{-j}.$$

Pairwise exchangeability means that we can swap null covariates with their knockoffs without changing the joint distribution of the original covariates  $\mathbf{W}$  and their knockoffs  $\tilde{\mathbf{W}}$ , conditional on the response  $Y$  [3]. Based on the above knockoff structure, in the case of a single source, the pairwise exchangeability between the null count features and their knockoffs is easily proven.

**Lemma 5.1 (Pairwise exchangeability)** *Take any subset  $S \subset \mathcal{H}_0$  of nulls. Then*

$$(\mathbf{W}, \tilde{\mathbf{W}}) \mid \mathbf{Y} \stackrel{d}{=} (\mathbf{W}, \tilde{\mathbf{W}})_{\text{swap}(S)} \mid \mathbf{Y}.$$

*Proof* [Lemma 5.1] Since  $\mathbf{Y}$ ’s marginal distribution is the same on both sides of the equation, it is equivalent to show that  $([\mathbf{W}, \tilde{\mathbf{W}}], \mathbf{Y}) \stackrel{d}{=} ([\mathbf{W}, \tilde{\mathbf{W}}]_{\text{swap}(S)}, \mathbf{Y})$ . Assume without loss of generality that  $S = \{1, 2, \dots, m\}$ . By row independence, it suffices to show that  $((W, \tilde{W}), Y) \stackrel{d}{=} ((W, \tilde{W})_{\text{swap}(S)}, Y)$ , where  $W$  (resp.  $Y$ ) is a row of  $\mathbf{W}$  (resp.

$Y$ ). Furthermore, since  $(W, \tilde{W}) \stackrel{d}{=} (W, \tilde{W})_{\text{swap}(S)}$ , it is only necessary to establish that

$$Y \mid (W, \tilde{W})_{\text{swap}(S)} \stackrel{d}{=} Y \mid (W, \tilde{W}). \quad (14)$$

Letting  $p_{Y|W}(y|w)$  be the conditional distribution of  $Y$ . Then the left-hand side of the above equation can be expressed as

$$p_{Y|(W, \tilde{W})_{\text{swap}(S)}}(y|(w, \tilde{w})) = p_{Y|(W, \tilde{W})}(y|(w, \tilde{w})_{\text{swap}(S)}) = p_{Y|W}(y|w'),$$

where  $w'_i = \tilde{w}_i$  if  $i \in S$  and  $w'_i = w_i$  otherwise. The second equality above comes from the fact that  $Y$  is conditionally independent of  $\tilde{W}$  by  $\tilde{W} \perp Y|W$ . Next, since  $Y$  and  $W_1$  are independent conditional on  $W_{2:p}$ , follows

$$p_{Y|W_{1:p}}(y|\tilde{w}_1, w'_{2:p}) = p_{Y|W_{2:p}}(y|w'_{2:p}) = p_{Y|W_{1:p}}(y|w_1, w'_{2:p}).$$

This shows that

$$Y \mid (W, \tilde{W})_{\text{swap}(S)} \stackrel{d}{=} Y \mid (W, \tilde{W})_{\text{swap}(S \setminus \{1\})}.$$

This argument can be repeated with the second feature, the third, and so on until  $S$  is empty. This proves 14.  $\square$

In fact, since the pairwise exchangeability property of  $(W, \tilde{W})$  holds conditionally on  $Y$  according to Lemma 5.1, the coin flipping property also holds conditionally on  $Y$ .

**Lemma 5.2 (Coin flipping)** *Conditionally on  $(|C_1|, \dots, |C_p|)$ , the signs of the null  $C_j$ s,  $j \in \mathcal{H}_0$ , are IID coin flips.*

*Proof* [Lemma 5.2] Let  $\epsilon = (\epsilon_1, \dots, \epsilon_p)$  be a sequence of independent random variables such that  $\epsilon_j = \pm 1$  with probability 0.5 if  $j \in \mathcal{H}_0$ , and  $\epsilon_j = 1$  otherwise. To prove the coin flipping property, it suffices to establish that

$$C \stackrel{d}{=} \epsilon \odot C,$$

where  $\epsilon \odot C = (\epsilon_1 C_1, \dots, \epsilon_p C_p)$ . Put  $S = \{j : \epsilon_j = -1\} \subset \mathcal{H}_0$ . Consider swapping variables in  $S$ :

$$C_{\text{swap}(S)} \triangleq f_{fs}\{(W, \tilde{W})_{\text{swap}(S)}, Y\}.$$

where  $f_{fs}$  represents the flip sign function. Hence, it follows from the flip sign property that  $C_{\text{swap}(S)} = \epsilon \odot C$ . And Lemma 5.1 implies that  $C_{\text{swap}(S)} \stackrel{d}{=} C$  since  $S \subset \mathcal{H}_0$ . These last two properties give result above.  $\square$

Therefore, the knockoffs constructed in this paper meet the requirements of the exchangeability and coin-flipping properties of Model-X knockoff methods. The subsequent theory can also refer to [3] to illustrate the FDR control results in the case of a single source. Furthermore, the knockoff construction process involves conditional randomization sampling, so the following lemma also holds.

**Lemma 5.3 (conditional randomization method [3])** *Under the null hypothesis  $Y \perp W_j \mid W_{-j}$ , any test statistic  $T = t(W_j, W_{-j}, Y)$  obeys*

$$T \mid (W_{-j}, Y) \stackrel{d}{=} \tilde{T} \mid (W_{-j}, Y),$$

where  $\tilde{T} = t(\tilde{W}_j, W_{-j}, Y)$ .

*Proof* [Lemma 5.3] To prove the claim, it suffices to show that  $W_j$  and  $\tilde{W}_j$  have the same distribution conditionally on  $(W_{-j}, Y)$ . This follows from

$$\tilde{W}_j \mid (Y, W_{-j}) \stackrel{d}{=} W_j \mid W_{-j} \stackrel{d}{=} W_j \mid (W_{-j}, Y).$$

The first equality comes from the definition of  $\tilde{W}_j$  while the second follows from the conditional independence of  $Y$  and  $W_j$ , which holds under the null.  $\square$

## 2. Theoretical Results for the Multi-Source Case

Define  $H_{0,kj}$  as the null hypothesis indicating that the feature  $W_{kj}$  is not associated with  $Y_k$  in the  $k$ -th experiment (i.e.,  $W_{kj} \perp Y_k \mid W_{-j}$  where  $W_{k,-j} := \{W_{k1}, \dots, W_{kp}\} \setminus W_{kj}$ ) [19]. Denote  $\mathcal{H}_k = \{j \in [p] : H_{0,kj} \text{ is true}\}$ , where  $[p] := \{1, \dots, p\}$ . Instead of testing the  $H_{0,kj}$ s, it is interested in testing the union null hypotheses

$$H_{0j} = \cup_{k=1}^K H_{0,kj}, \text{ for } j \in [p].$$

Define  $\mathcal{S} = \{j \in [p] : H_{0j} \text{ is false}\}$  and  $\mathcal{H} = \mathcal{S}^c = \cup_{k=1}^K \mathcal{H}_k = \{j \in [p] : H_{0j} \text{ is true}\}$ . The aim is to develop a selection procedure returning a selection set  $s \in [p]$  with a controlled FDR, which is the expected false discovery proportion (FDP):

$$FDR(\hat{S}) = \mathbb{E} \left[ FDP(\hat{S}) \right] = \mathbb{E} \left[ \frac{|\hat{S} \cap \mathcal{H}|}{|\hat{S}| \vee 1} \right].$$

The key step in proving the control of the FDR is that the null statistics  $C_j$ 's have signs distributed as i.i.d. coin flips (even conditionally on  $y$ ). As for the knockoff-based methods, this property effectively guarantees that for all  $j \in \mathcal{H}$ , there are equal probabilities of selecting the feature and its knockoff copy. As Lemma 1 shows, the single-source knockoff satisfies pairwise exchangeability. Thus, the following proofs of Lemma 5.4 and Theorem 5.5 are the same as those of Theorems 1 and Lemma 1 in [19], and therefore, they have already been proven. Similarly, the proof procedure for the FDR control based on the DE statistic is analogous to that in [39] and is therefore omitted.

**Lemma 5.4 (i.i.d. signs for the nulls)** *Let  $\mathbf{C} = f_{OSFF}([\mathbf{Z}_1, \tilde{\mathbf{Z}}_1], \dots, [\mathbf{Z}_K, \tilde{\mathbf{Z}}_K])$ . Let  $\boldsymbol{\epsilon} \in \{\pm 1\}^p$  be a sign sequence independent of  $\mathbf{C}$  with  $\epsilon_j = 1$  for all  $j \in \mathcal{S}$  and  $\epsilon_j \sim \{\pm 1\}$  for all  $j \in \mathcal{H}$ . Then,  $(C_1, \dots, C_p) \stackrel{d}{=} (C_1 \cdot \epsilon_1, \dots, C_p \cdot \epsilon_p)$ .*

*Proof* [Lemma 5.4] For any  $S \subseteq \mathcal{H}$ , where  $S = \cup_{k=1}^K S_k$ ,  $S_k \subseteq \mathcal{H}_k$  for  $k \in [K]$ , and  $S_{k_1} \cap S_{k_2} = \emptyset$  for all  $k_1 \neq k_2$ . In particular, let  $S_k = S \cap \mathcal{H}_k \cap (\cup_{j=1}^{k-1} \mathcal{H}_j)^c$ . Since  $S_k \subseteq \mathcal{H}_k$ , any statistics  $[\mathbf{Z}_k, \tilde{\mathbf{Z}}_k] = f_{fs}([\mathbf{X}^k, \tilde{\mathbf{X}}^k], \mathbf{Y}_k)$ , where the knockoffs satisfy  $[\mathbf{Z}_k, \tilde{\mathbf{Z}}_k] \stackrel{d}{=} [\mathbf{Z}_k, \tilde{\mathbf{Z}}_k]_{\text{Swap}(S_k)}$ . By the mutually independent between  $[\mathbf{Z}_1, \tilde{\mathbf{Z}}_1], \dots, [\mathbf{Z}_K, \tilde{\mathbf{Z}}_K]$ , it follows that

$$f([\mathbf{Z}_1, \tilde{\mathbf{Z}}_1]_{\text{Swap}(S_1)}, \dots, [\mathbf{Z}_K, \tilde{\mathbf{Z}}_K]_{\text{Swap}(S_K)}) \stackrel{d}{=} f([\mathbf{Z}_1, \tilde{\mathbf{Z}}_1], \dots, [\mathbf{Z}_K, \tilde{\mathbf{Z}}_K]).$$

Using the definition of the OSFF:

$$\begin{aligned} & f([\mathbf{Z}_1, \tilde{\mathbf{Z}}_1]_{\text{Swap}(S_1)}, [\mathbf{Z}_2, \tilde{\mathbf{Z}}_2]_{\text{Swap}(S_2)}, \dots, [\mathbf{Z}_K, \tilde{\mathbf{Z}}_K]_{\text{Swap}(S_K)}) \\ &= f([\mathbf{Z}_1, \tilde{\mathbf{Z}}_1], [\mathbf{Z}_2, \tilde{\mathbf{Z}}_2]_{\text{Swap}(S_2)}, \dots, [\mathbf{Z}_K, \tilde{\mathbf{Z}}_K]_{\text{Swap}(S_K)}) \odot \boldsymbol{\epsilon}(S_1) \\ &= \dots \\ &= f([\mathbf{Z}_1, \tilde{\mathbf{Z}}_1], [\mathbf{Z}_2, \tilde{\mathbf{Z}}_2], \dots, [\mathbf{Z}_K, \tilde{\mathbf{Z}}_K]) \odot_{k=1}^K \boldsymbol{\epsilon}(S_k) \\ &= f([\mathbf{Z}_1, \tilde{\mathbf{Z}}_1], [\mathbf{Z}_2, \tilde{\mathbf{Z}}_2], \dots, [\mathbf{Z}_K, \tilde{\mathbf{Z}}_K]) \odot \boldsymbol{\epsilon}(S). \end{aligned}$$

Thus, for any  $S \subseteq \mathcal{H}$ , the following is obtained

$$\mathbf{C} = f([\mathbf{Z}_1, \tilde{\mathbf{Z}}_1], \dots, [\mathbf{Z}_K, \tilde{\mathbf{Z}}_K]) \stackrel{d}{=} f([\mathbf{Z}_1, \tilde{\mathbf{Z}}_1], \dots, [\mathbf{Z}_K, \tilde{\mathbf{Z}}_K]) \odot \boldsymbol{\epsilon}(S) = \mathbf{C} \odot \boldsymbol{\epsilon}(S).$$

Therefore, let  $S = \{j : \epsilon_j = -1\} \subseteq \mathcal{H}$ , it follows that

$$(C_1, \dots, C_p) \stackrel{d}{=} (C_1 \cdot \epsilon_1, \dots, C_p \cdot \epsilon_p).$$

□

**Theorem 5.5** *With the individual experiments satisfying the the Model-X knockoff model settings (Lemma 5.1), the Simultaneous knockoff procedure for multi-source count data*

$$\hat{S} = \{j : C_j \geq \tau\}, \text{ where } \tau = \min \left\{ t \in \mathcal{C}_+ : \frac{\#\{j : C_j \leq -t\}}{\#\{j : C_j \geq t\} \vee 1} \leq q \right\}.$$

*controls the modified FDR defined as*

$$\text{mFDR} = \mathbb{E} \left[ \frac{|\hat{S} \cap \mathcal{H}|}{|\hat{S}| + 1/q} \right] \leq q,$$

*where  $q$  is the target FDR level (or  $\tau = \infty$  if the set above is empty),  $\mathcal{C}_+ = \{|C_j| : |C_j| > 0\}$  and  $\mathcal{H}$  is the union null set as defined above.*

*The Simultaneous knockoff+ procedure for multi-source count data*

$$\hat{S}_+ = \{j : C_j \geq \tau_+\}, \text{ where } \tau_+ = \min \left\{ t \in \mathcal{C}_+ : \frac{1 + \#\{j : C_j \leq -t\}}{\#\{j : C_j \geq t\} \vee 1} \leq q \right\}.$$

controls the usual FDR

$$\mathbb{E} \left[ \frac{|\widehat{S}_+ \cap \mathcal{H}|}{|\widehat{S}_+| \vee 1} \right] \leq q.$$

*Proof* [Theorem 5.5] Let  $m = \#\{j : W_j \neq 0\}$  and assume without loss of generality that  $|W_1| \geq |W_2| \geq \dots \geq |W_m| > 0$ . Define p-values  $p_j = 1$  if  $W_j < 0$  and  $p_j = 1/2$  if  $W_j > 0$ , then Lemma 5.4 implies that null p-values are *i.i.d.* with  $p_j \geq \text{Unif}[0, 1]$  and are independent from nonnulls.

First, the result for  $V = \#\{j \leq \widehat{k}_+ : p_j \leq 1/2, j \in \mathcal{H}\}$  and  $R = \#\{j \leq \widehat{k}_+ : p_j \leq 1/2\}$  is shown, where  $\widehat{k}_+$  satisfies  $|W_{\widehat{k}_+}| = \tau_+$ . Then

$$\begin{aligned} \mathbb{E} \left[ \frac{V}{R \vee 1} \right] &= \mathbb{E} \left[ \frac{V}{R \vee 1} \mathbb{1}_{\widehat{k}_+ > 0} \right] \\ &= \mathbb{E} \left[ \frac{\#\{j \leq \widehat{k}_+ : p_j \leq 1/2, j \in \mathcal{H}\}}{1 + \#\{j \leq \widehat{k}_+ : p_j > 1/2, j \in \mathcal{H}\}} \left( \frac{1 + \#\{j \leq \widehat{k}_+ : p_j > 1/2, j \in \mathcal{H}\}}{\#\{j \leq \widehat{k}_+ : p_j \leq 1/2\} \vee 1} \right) \mathbb{1}_{\widehat{k}_+ > 0} \right] \\ &\leq \mathbb{E} \left[ \frac{\#\{j \leq \widehat{k}_+ : p_j \leq 1/2, j \in \mathcal{H}\}}{1 + \#\{j \leq \widehat{k}_+ : p_j > 1/2, j \in \mathcal{H}\}} \right] q \leq q, \end{aligned}$$

where the first inequality holds by the definition of  $\widehat{k}_+$  and the second inequality holds by Lemma 5.6.

Similarly, for the knockoff threshold,  $V = \#\{j \leq \widehat{k}_0 : p_j \leq 1/2, j \in \mathcal{H}\}$  and  $R = \#\{j \leq \widehat{k}_0 : p_j \leq 1/2\}$ , where  $\widehat{k}_0$  satisfies that  $|W_{\widehat{k}_0}| = \tau$ , then

$$\begin{aligned} \mathbb{E} \left[ \frac{V}{R + q^{-1}} \right] &= \mathbb{E} \left[ \frac{\#\{j \leq \widehat{k}_0 : p_j \leq 1/2, j \in \mathcal{H}\}}{1 + \#\{j \leq \widehat{k}_0 : p_j > 1/2, j \in \mathcal{H}\}} \left( \frac{1 + \#\{j \leq \widehat{k}_0 : p_j > 1/2, j \in \mathcal{H}\}}{\#\{j \leq \widehat{k}_0 : p_j \leq 1/2\} + q^{-1}} \right) \mathbb{1}_{\widehat{k}_0 > 0} \right] \\ &\leq \mathbb{E} \left[ \frac{\#\{j \leq \widehat{k}_0 : p_j \leq 1/2, j \in \mathcal{H}\}}{1 + \#\{j \leq \widehat{k}_0 : p_j > 1/2, j \in \mathcal{H}\}} \right] q \leq q, \end{aligned}$$

where the first inequality holds by the definition of  $\widehat{k}_0$  and the second inequality holds by Lemma 5.6.  $\square$

**Lemma 5.6** For  $k = m, m-1, \dots, 1, 0$ , put  $V^+(k) = \#\{j : 1 \leq j \leq k, p_j \leq 1/2, j \in \mathcal{H}\}$  and  $V^-(k) = \#\{j : 1 \leq j \leq k, p_j > 1/2, j \in \mathcal{H}\}$  with the convention that  $V^\pm(0) = 0$ . Let  $\mathcal{F}_k$  be the filtration defined by knowing all the non-null p-values, as well as  $V^\pm(k')$  for all  $k' \geq k$ . Then the process  $M(k) = \frac{V^+(k)}{1+V^-(k)}$  is a super-martingale running backward in time with respect to  $\mathcal{F}_k$ . For any fixed  $q$ ,  $\widehat{k} = \widehat{k}_+$  or  $\widehat{k} = \widehat{k}_0$  as defined in the proof of theorem 1 are stopping times, and as consequences

$$\mathbb{E} \left[ \frac{\#\{j \leq \widehat{k} : p_j \leq 1/2, j \in \mathcal{H}\}}{1 + \#\{j \leq \widehat{k} : p_j > 1/2, j \in \mathcal{H}\}} \right] \leq 1.$$

*Proof* [Lemma 5.6] The proof follows the same reasoning as Lemma B3 in [19] and is therefore omitted.  $\square$

## 5.2 Simulation results

### 5.2.1 Simulation settings

Some other generic Settings: assuming that the  $j$ -th count variable has a corresponding zero inflation probability  $\pi_j$ . When it is related to  $\mathbf{Y}_k$ , its two distributions have different zero inflation probabilities  $\pi_{j1}, \pi_{j2}$ . The covariate  $\mathbf{X}_{n_k \times d}$  associated with  $\mathbf{W}_k$  follows a normal distribution, that is,  $\mathbf{X} \sim N_d(\mathbf{0}, \Sigma)$ , where  $\Sigma = (\rho_{i,j})_{d \times d}$ ,  $\rho_{i,j} = 0.1^{|i-j|}$ . Also, we set the parameters of the link function as  $\beta_{j,0} = \beta_{j,0}^* = 1$ ,  $\beta_j = \beta_j^* = 0.1, j \in [p_1]$  or  $\beta_j = \beta_j^* = 0, j \in [p_2]$ , respectively. Based on these parameter values, we can simply calculate the corresponding  $\lambda_j, \theta_j$ .

We chose two ways to generate simulated count data: copula-based and non-copula-based:

- Copula-based: This process is similar to the synthetic null data generation.
  1. Partition of variables: it is divided into two groups of variables  $\mathbf{p}_{\pi_1}$ ,  $\mathbf{p}_{\pi_2}$ , where  $\pi_1 \leq 0.8$  and  $\pi_2 > 0.8$ . The count data of  $\mathbf{p}_{\pi_1}$  continues to generate data based on copula methods, while  $\mathbf{p}_{\pi_2}$  directly generated data based on the non-copula method.
  2. First, generate  $\mathbf{Z} \sim N_{p_{\pi_1}}(\mathbf{0}, \mathbf{R})$ ,  $\mathbf{R} = (r_{i,j})_{p_{\pi_1} \times p_{\pi_1}}$ ,  $r_{i,j} = 0.5^{|i-j|}$ , and then distribution function values  $\Phi(\mathbf{Z})$  of the ZIPG distribution are obtained based on the inverse transformation of the standard normal distribution;
  3. Based on the distribution  $P_{\text{ZIPG}}(\mathbf{W}; \lambda, \theta, \pi_j)$  and the zero inflation probability  $\pi_j$ , the CDF value of the PG distribution is obtained, and the corresponding count value  $\mathbf{W}_j$  is directly obtained through the quantile function of the PG distribution.
- Non-copula-based: For each variable  $j$ , given the values of  $\lambda_j$ ,  $\theta_j$  of PG or NB distribution, we can sample directly from the corresponding distribution to get a count vector  $\mathbf{W}_j$  of length  $n_k$ .

At the same time, some knockoff-related construction models are used for comparison with the proposed method:

- Model-X knockoff: a method for selecting a high-dimensional control variable. This paper not only construct knockoff based on this method, but also uses functions in R package knockoff to build test statistics.
- scDesign2 [27]: a transparent simulator that generates count data with variables correlations captured. This method is also based on the copula statistical framework, and its marginal distribution has multiple choices (Poisson, ZIP, NB, and ZINB), and ZINB is mainly selected in this paper.

### 5.2.2 Results of different methods and strategies

This paper aims to compare the outcomes of three variable set selection strategies: Intersection, Pooling, and Simultaneous (abbreviated as Inter, Pool, SK). For constructing knockoffs, the paper employs Model-X knockoff, scDesign2, and the ZIPG distribution specified by the Gaussian copula (abbreviated as MX, ZINB, and ZIPG). Additionally, this study utilizes clusterDE, glmnet, and random forest to compute test statistics (abbreviated as DE, GLM, and RF, respectively) for comparison purposes. Therefore, this paper focuses on evaluating the results of several implementation approaches of the ZIPG-SK method, namely ZIPG-SK-DE, ZIPG-SK-GLM, and ZIPG-SK-RF, and comparing them with the outcomes obtained from other methods.

In a preliminary analysis, we consider the  $K = 2$  first. We set the first 10% count features is significantly correlated with  $Y$  and the FDR control value for different methods to 0.2. The results of there different methods (MX, ZINB, and simul) are mainly compared, and the control results and power of FDR are compared according to different ways of calculating statistics (DE, GLM, RF) and ways of obtaining selection sets (Intersection, Pooling Simultaneous).

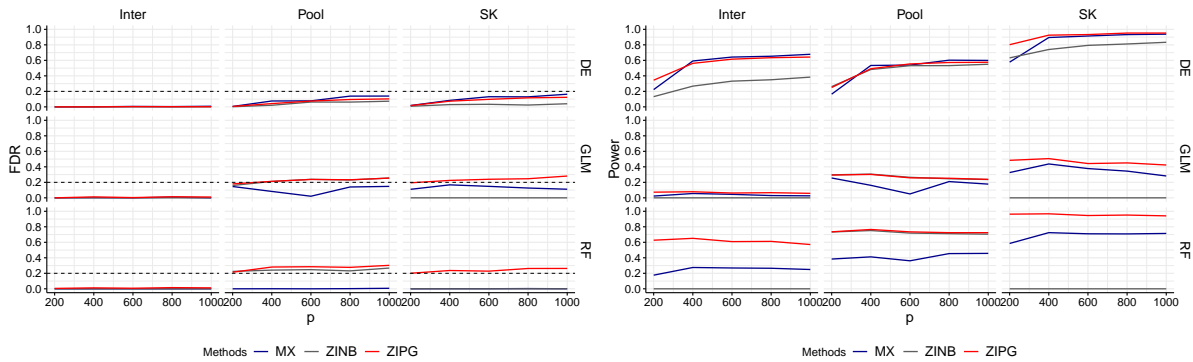


Figure 5: The power and the FDR results of copula-based simulation data. ZIPG, ZINB, and MX represent the data generation methods, while DE, GLM, and RF represent the methods used for test statistic calculation. The Inter, Pool, and SK represent different strategies of variable set selection, respectively. (The methodology descriptions for the subsequent figures are identical to the one provided here.)

Figure 5 presents the results of FDR control and power for 50 experiments under the different methods and strategies described above for different variable cases. Each data source consists of a sample size of 400, with variable ranges varying from 200 to 1000. The left figure displays the FDR results, indicating a generally stable FDR curve across different variable dimensions. However, the Intersection strategy exhibits poor FDR control, with values either

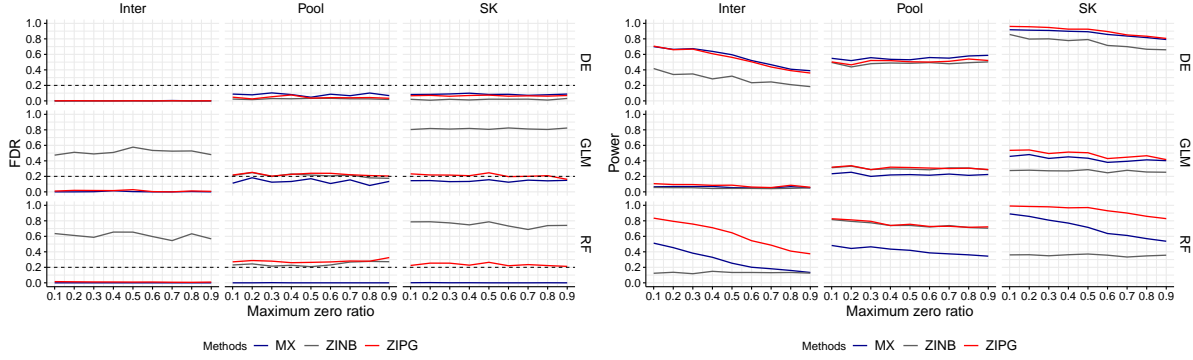


Figure 6: The power and the FDR results of different maximum zero proportions. ZIPG, ZINB, and MX represent the data generation methods, while DE, GLM, and RF represent the methods used for test statistic calculation. The Inter, Pool, and SK represent different strategies of variable set selection, respectively. (The methodology descriptions for the subsequent figures are identical to the one provided here.)

approaching 0 (too low) or exceeding 0.4 (too high). Comparatively, the Pooling and Simultaneous strategies yield better FDR control. Overall, all three methods can maintain FDR at around 0.2 in most cases. Notably, the method proposed in this paper (ZIPG-SK: ZIPG-SK-DE, ZIPG-SK-GLM, and ZIPG-SK-RF) consistently outperforms the other methods across all 6 subgraphs. On the other hand, the MX and ZINB methods fail to adequately control FDR in certain scenarios. For instance, when obtaining the selection set in Simultaneous mode and calculating statistics based on RF (SK-RF), the konckoff method exhibits excessively low FDR control, while the ZINB method demonstrates excessively high FDR control. The right figure presents the power results, indicating that the method proposed in this paper (red line) consistently achieves the highest power. However, it is worth noting that the power of GLM statistics calculations is significantly lower compared to the other two methods (DE, RF). The former generally remains below 0.5, while the latter two methods in this paper consistently exceed 0.8. This discrepancy may be attributed to the non-linear relationship between count data and label  $Y$  in the simulated data.

### 5.2.3 Results of two common challenges in multi-source count data

This paper addresses two common challenges encountered in multi-source count data analysis. Firstly, count data often exhibit an abundance of zeros, and secondly, the true selection sets of data from different sources in multi-source data are frequently inconsistent.

Figure 6 illustrates the results of FDR and power analysis while considering the maximum zero proportion in count data, ranging from 0.1 to 0.9. The sample size is also 400, and there are 1000 variables. The maximum zero proportion represents the highest proportion of zeros that may occur in the count data of a specific variable. Specifically, the zero inflation probability ( $\pi_j$ ) for the  $j$ -th count variable is uniformly sampled from the interval between 0 and the maximum zero proportion. It can be observed that FDR results remain relatively stable across different maximum zero proportions. Similar to the findings in Figure 5, the proposed method in this paper exhibits the most effective FDR control, indicating its robustness to the influence of maximum zero proportions. However, the power results in Figure 6 show a slight downward trend as the maximum zero proportion increases.

Figure 7 presents the FDR and power results for the two datasets ( $K=2$ ) with varying levels of significant variable differences (diff) ranging from 0 to 60. It is apparent that the FDR controlled by the three methods increases with the growth of diff. The Pooling strategy demonstrates poor performance, deviating substantially from the desired FDR of 0.2. Comparatively, the method proposed in this paper consistently maintains desirable FDR control across the different scenarios, while also achieving superior power results compared to the other two methods.

### 5.2.4 Results of non-copula-based scenario and the case with $K = 3$

Figure 8 displays the results obtained from data generation without copula. It is evident that the method proposed in this paper remains consistent with previous findings and demonstrates superiority over other methods in this scenario. In Figure 9, which illustrates the case of a multi-source dataset with  $K=3$ , the superiority of the method in this paper persists. Particularly, its power is notably higher when controlling the False Discovery Rate (FDR).

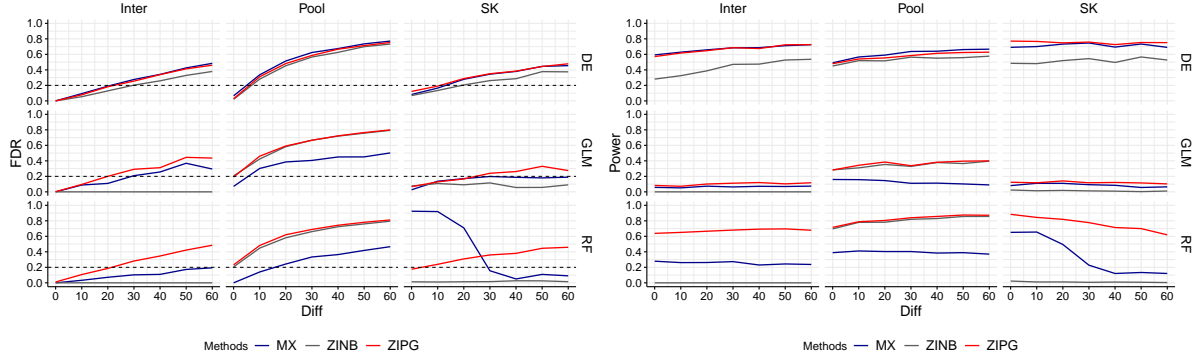


Figure 7: The FDR and power results for two datasets ( $K=2$ ) with different number of significant variable differences (Diff).

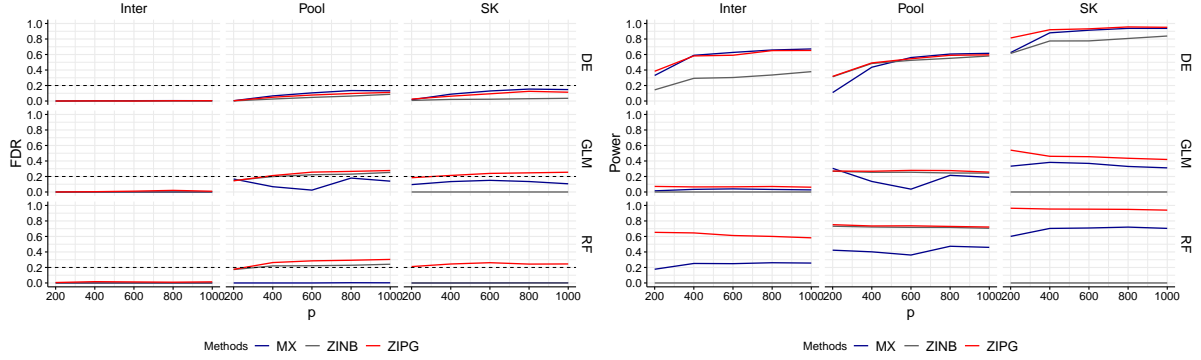


Figure 8: The power and the FDR results of non-copula-based scenario.

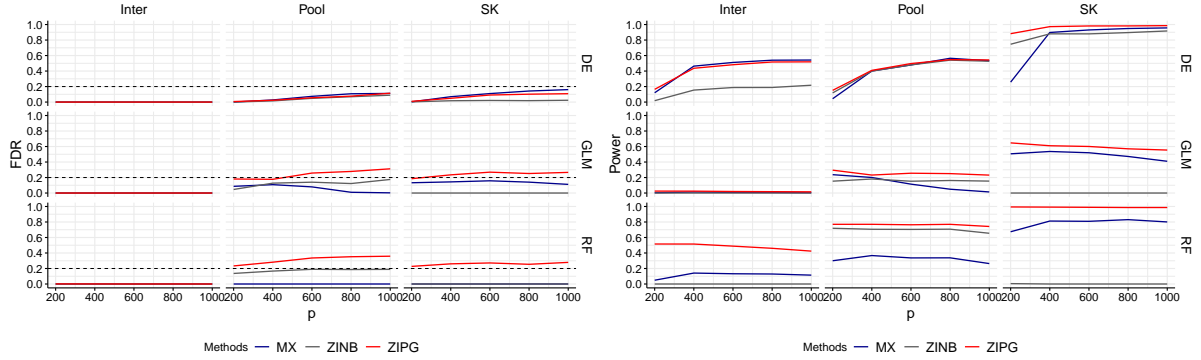


Figure 9: The power and the FDR for the settings when  $K = 3$ .

### 5.2.5 Simulation results based on the aggregate algorithm

Figure 10 presents the results of FDR control and power for different aggregating modalities. In the figure, '1' represents the aggregation of test statistics, '11' represents the calculation of filter statistics based on the Simultaneous method, and '12' represents the calculation of filter statistics based on the Fisher combination p-value method. '2' represents the aggregation of other filter statistics. It can be observed that the method based on '12' performs relatively well; however, the results of other aggregating methods still need improvement.

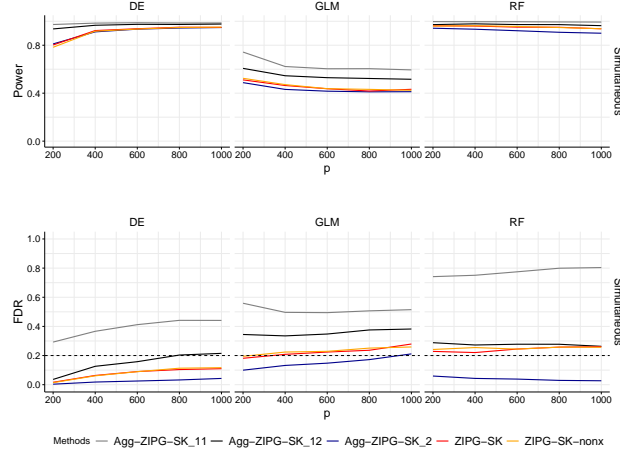


Figure 10: The power and the FDR for the settings based on the aggregate algorithm.

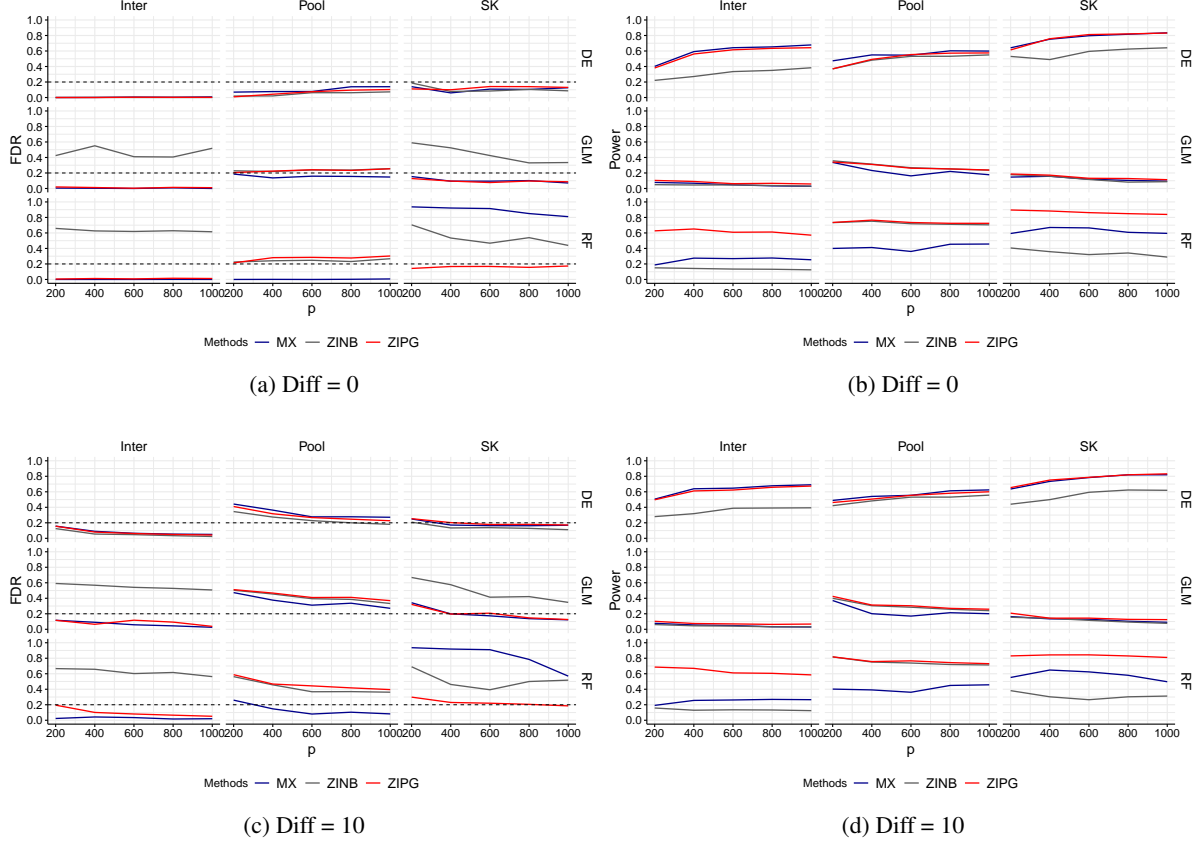


Figure 11: The power and the FDR for the settings based on Direct Diff Dot product (OSFF) when Diff = 0 and 10.

### 5.2.6 The simulation results based on other OSFF cases

Figure 11 displays the results of the OSFF function based on the Direct Diff Dot product, while also considering the case of the significant variable set difference (Diff = 0 and 10) for the two datasets. The analysis process is based on consistency with the paper, essentially demonstrating that the method proposed in this paper outperforms other methods in processing count data.



Table 1: Size and characteristics of the seven datasets.

BioProject (ref.)	Groups (n)	Age ( <i>average</i> $\pm$ <i>s.d.</i> )	BMI ( <i>average</i> $\pm$ <i>s.d.</i> )	Sex <i>F</i> (%)/ <i>M</i> (%)	Country
PRJEB7774 [40]	CRC(46)	67.1 $\pm$ 10.9	26.5 $\pm$ 3.5	39.1/60.9	Austria
	HC(63) <sup>a</sup>	67.1 $\pm$ 6.4	27.6 $\pm$ 3.8	41.3/58.7	
PRJEB10878 [41]	CRC(74)	66.0 $\pm$ 10.6	24.0 $\pm$ 3.2	36.5/63.5	China
	HC(53) <sup>a</sup>	61.8 $\pm$ 5.7	23.5 $\pm$ 3.0	37.7/62.3	
PRJEB6070 [42]	CRC(51) <sup>a</sup>	66.8 $\pm$ 10.9	25.6 $\pm$ 5.2	45.1/54.9	France
	HC(59) <sup>a</sup>	60.6 $\pm$ 11.6	24.7 $\pm$ 3.2	54.2/45.8	
PRJEB27928 [43]	CRC(60) <sup>a</sup>	63.5 $\pm$ 12.6	26.2 $\pm$ 4.0	40.0/60.0	Germany
	HC(60) <sup>a</sup>	57.6 $\pm$ 11.1	24.9 $\pm$ 3.2	46.7/53.3	
PRJDB4176 [44]	CRC(225) <sup>a</sup>	61.8 $\pm$ 10.5	22.7 $\pm$ 3.1	41.8/58.2	Japan
	HC(222) <sup>a</sup>	61.1 $\pm$ 12.3	22.9 $\pm$ 3.3	41.4/58.6	
PRJEB12449 [45]	CRC(49) <sup>a</sup>	61.0 $\pm$ 13.4	24.9 $\pm$ 4.2	26.5/73.5	USA
	HC(52)	61.2 $\pm$ 11	25.3 $\pm$ 4.3	28.8/71.2	
<b>Total</b>	<b>CRC(505)</b>	<b>63.5 <math>\pm</math> 11.4</b>	<b>24.2 <math>\pm</math> 3.9</b>	<b>39.4/60.6</b>	
	<b>HC(509)</b>	<b>61.4 <math>\pm</math> 11.0</b>	<b>24.2 <math>\pm</math> 3.7</b>	<b>41.8/58.2</b>	

<sup>a</sup> Due to metadata and/or sequence-processing issues, the numbers presented herein may differ from those originally reported in the respective articles. The last two rows, highlighted in bold, provide the combined statistics for all cohorts above and include information regarding the number of samples for each condition.

### 5.3 Real data analysis of CRC

#### 5.3.1 Dataset details and characteristics

The details and characteristics of six datasets have been summarized in Table 1. The dataset includes a total of 1064 individuals, among which there are 505 CRC patients and 509 healthy controls (HC), and encompasses 845 distinct gut microbial species.

#### 5.3.2 Classification diagnosis of CRC

In addition, we perform a classification diagnosis of CRC based on the results of gut microbiota selection using various methods. Taking into account differences in data sources and sample sizes, we employ distinct strategies to construct test sets, facilitating comparative analysis. Among these, "5-fold CV" pertains to cross-validating the pooling samples 20 times; "Sample size" signifies that samples of the same size are randomly chosen from datasets across various regions to establish a test set, with the remaining samples forming a training set, a process repeated 20 times. "Data sources" entail using different regions as test sets and the remaining regions as training sets.

Table 2 presents the performance metrics of different classification methods for the four variable selection modalities of gut microbes. It is evident that, in comparison with coda-lasso-CV, the number of intestinal microorganisms identified by the method presented in this study is notably diminished. Despite this reduction, the results exhibit relatively improved performance in metrics such as AUC. Both the method proposed in this study and clr-lasso-CV select six types of intestinal microorganisms. Moreover, no significant disparities are observed in AUC and other indicators under varying conditions when compared to the clr-lasso-CV method. The results indicate that the classification accuracy of the four methods is comparable. Despite selecting relatively few intestinal microorganisms, the proposed method demonstrates good effectiveness in classification tasks, thereby confirming its validity.

#### 5.3.3 Real data results based on the aggregate algorithm

Figure 12 presents the selection of real data using the aggregation algorithm. Variable selection is performed directly on all data samples. The results indicate that the outcomes based on different selection strategies are consistent with the findings in the paper, and the selection of intestinal microorganisms using the Simultaneous method is relatively reasonable. Furthermore, when comparing different aggregation algorithms to the original method, the results for most variables are largely similar, except in a few cases. This suggests that the original method is sufficiently effective in this paper. Consequently, the aggregate algorithm is not considered in this paper or subsequent analyses.

Table 2: Classification diagnosis of CRC.

Testsets	classification	Selection	NumVarSel	TPR	FPR	ACC	AUC
5-fold CV	SVM	ZIPG-SK-DE	6	0.7643	0.3530	0.6815	0.7318
		ZIPG-SK-GLM	6	0.8749	0.3703	0.6832	<u>0.7403</u>
		clr-lasso-CV	6	0.7012	0.3004	0.6940	<b>0.7450</b>
		coda-lasso-CV	60	0.6537	0.3180	0.6634	0.7191
		ZIPG-SK-DE	6	0.7633	0.3089	0.7164	0.7481
	RF	ZIPG-SK-GLM	6	0.9067	0.3758	0.6846	<b>0.8056</b>
		clr-lasso-CV	6	0.6807	0.3013	0.6865	<u>0.7663</u>
		coda-lasso-CV	60	0.6658	0.2800	0.6867	<u>0.7185</u>
		ZIPG-SK-DE	6	0.7552	0.3456	0.6891	0.7362
		ZIPG-SK-GLM	6	0.8793	0.3679	0.6887	<b>0.7446</b>
Sample size	SVM	clr-lasso-CV	6	0.6983	0.2934	0.6964	<u>0.7412</u>
		coda-lasso-CV	60	0.6589	0.3130	0.6704	0.7217
		ZIPG-SK-DE	6	0.7613	0.3050	0.7196	0.7522
		ZIPG-SK-GLM	6	0.9017	0.3718	0.6909	<b>0.8050</b>
		clr-lasso-CV	6	0.6772	0.2970	0.6863	<u>0.7637</u>
	RF	coda-lasso-CV	60	0.6644	0.2754	0.6876	<u>0.7203</u>
		ZIPG-SK-DE	6	0.7399	0.3598	0.6702	0.7192
		ZIPG-SK-GLM	6	0.8218	0.3701	0.6741	<u>0.7334</u>
		clr-lasso-CV	6	0.7210	0.2887	0.7067	<b>0.7389</b>
		coda-lasso-CV	60	0.6623	0.3281	0.6630	0.7086
Data sources (Regions)	RF	ZIPG-SK-DE	6	0.7624	0.3124	0.7125	0.7411
		ZIPG-SK-GLM	6	0.8923	0.3827	0.6766	<b>0.7968</b>
		clr-lasso-CV	6	0.6768	0.3052	0.6804	<u>0.7689</u>
		coda-lasso-CV	60	0.6796	0.2620	0.7001	<u>0.7150</u>

'NumVarSel' represents the number of selected variables. Two widely-used machine learning models (i.e., SVM and Random Forest) are employed. Four evaluation metrics, namely True Positive Rate (TPR), False Positive Rate (FPR), Accuracy (ACC), and Area Under the Curve (AUC), are utilized to assess the performance of the classifiers. The bold text denotes the optimal result between the methods under comparison in this study, while the underlined text indicates suboptimal results.

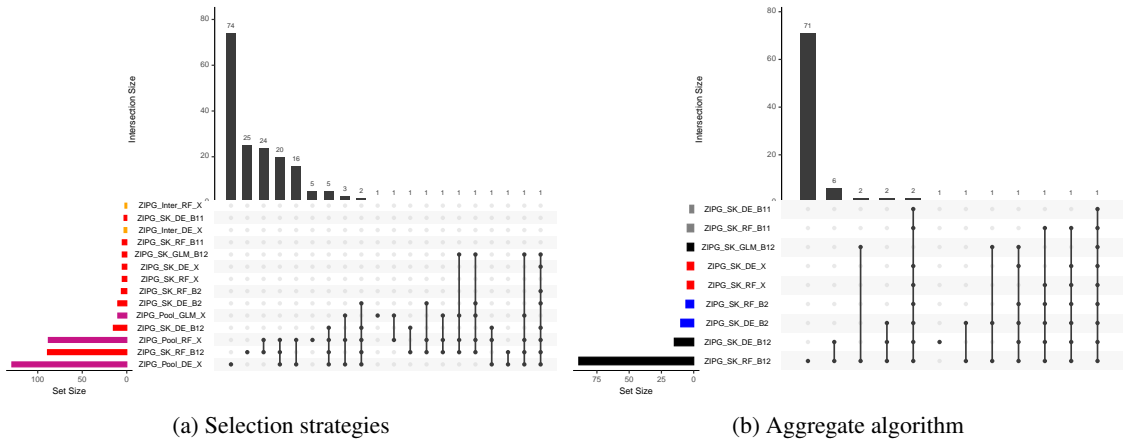


Figure 12: The selection results of real data using the aggregate algorithm. Both figures illustrate the upset plot of variable selection based on the ZIPG method applied to real data. The above panel focuses on the outcomes under different selection strategies (Inter, Pool, SK), while the below panel examines the results using various aggregate algorithm (B11, B12, B2).

### 5.3.4 Real data results based on other OSFF

Figure 13 displays the number and overlap of selected gut microbial variables under different methods and strategies based on Direct Diff Sum (OSFF). Although there are some differences observed in the results presented in this paper, they generally remain consistent across most methods.

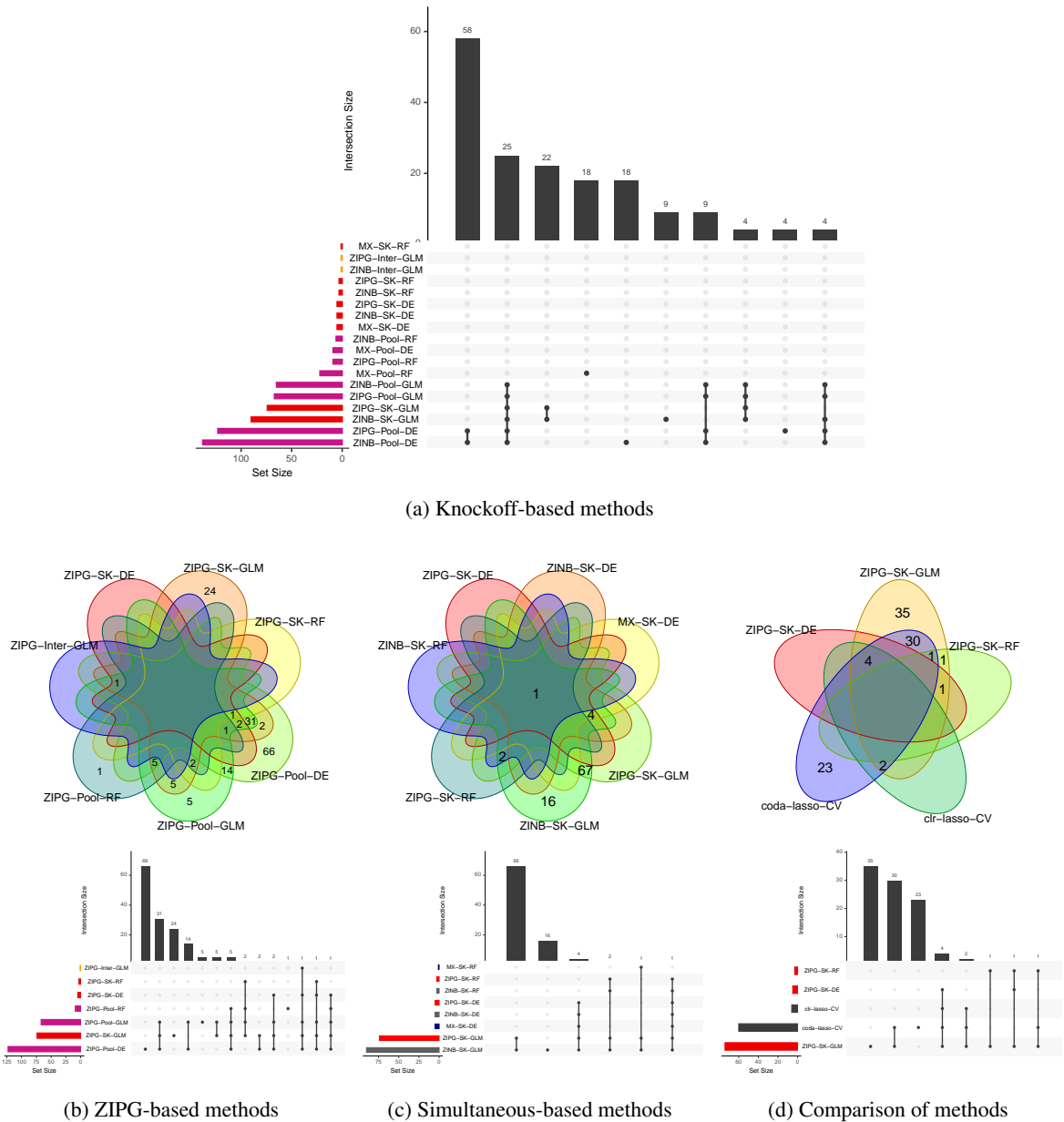
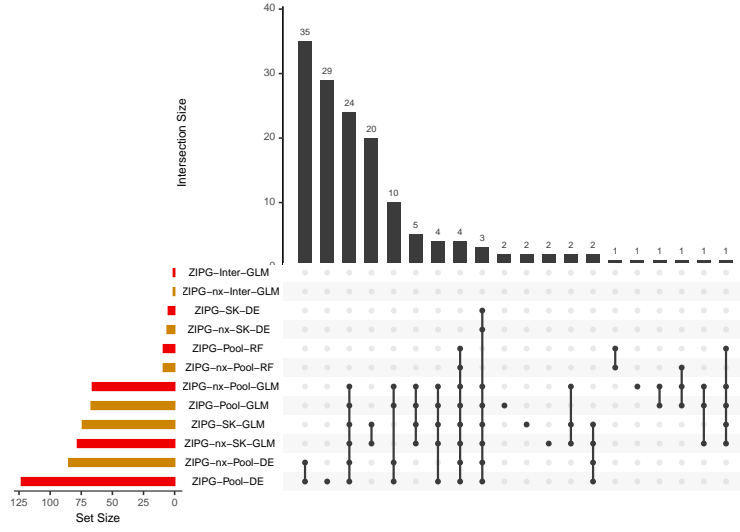
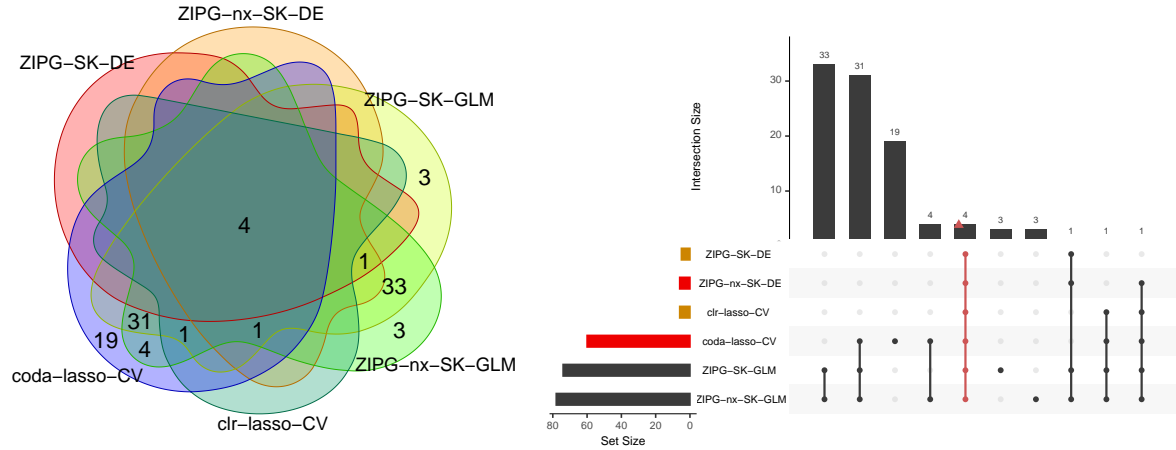


Figure 13: The number and overlap of selected gut microbial variables under different methods and strategies based on Direct Diff Sum (OSFF). Panel (a) displays the results obtained using various method strategies explored in this paper. ZIPG, ZINB, and MX represent the data generation methods, while DE, GLM, and RF represent the methods used for test statistic calculation. The letters I, P, and S signify the Intersection, Pooling, and Simultaneous strategies of variable set selection, respectively. Panel (b) showcases the outcomes of the ZIPG-based generation method. Panel (c) presents the results obtained using the Simultaneous strategy. Panel (d) presents a comparison between the final method (ZIPG-SK-DE, ZIPG-GLM-S, ZIPG-RF-S) and the two penalty regression methods discussed in this paper.

Figure 14 shows the results of variable selection with or without the use of covariates (clinical factors), and the variables selected under different methods are essentially the same. This may indicate that certain covariates not obviously related to gut microbiota have little influence on the final variable selection results.



(a) The results based on ZIPG and ZIPG-nx



(d) Comparison between ZIPG and ZIPG-nx

Figure 14: The number and overlap of selected gut microbial variables under different methods and strategies. Panel (a) displays the results obtained based on ZIPG and ZIPG-nx. ZIPG and ZIPG-nx represent the data generation methods, the latter not based on covariates. Panel (b) presents a comparison between the final method (ZIPG and ZIPG-nx) and the two penalty regression methods.

## 5.4 Real data analysis of T2D

### 5.4.1 Dataset details and characteristics

The T2D dataset comprises thousands of human islet cells obtained from six healthy individuals and four T2D donors, with variations in BMI and age detailed in Table 3 [22]. The dataset comprises 2032 cells, encompassing various subpopulations like alpha cells and acinar cells, and provides count data for 30415 genes. We choose islet cells that include HbA1c information, as depicted in Table 4. Simultaneously, preprocessing is carried out utilizing the R package Seurat, leading to the identification of 2000 highly variable genes.

This section focuses on the differentially expressed genes (DEGs) across various cell types in healthy individuals and patients with T2D, encompassing six distinct cell types. In this analysis, we explore the DEGs across multiple cell types, including all six cell types, three cell types ( $\alpha$  cells,  $\beta$  cells, and  $\delta$  cells), and two cell types ( $\alpha$  cells and  $\beta$  cells), respectively.

Table 3: Table of donor information (HbA1c, glycated hemoglobin).

Donor	Sex	Age	BMI	HbA1c
H1	male	43	30.8	5.00%
H2	male	25	24.7	5.30%
H3	female	48	35	5.70%
H4	male	22	32.9	5.40%
H5	male	27	31.8	N/D
H6	male	23	21.5	5.50%
T2D1	male	57	24	7.00%
T2D2	female	37	39.6	7.30%
T2D3	male	52	34.4	7.70%
T2D4	female	55	29.8	7.40%

Table 4: Number of islet cell subsets

	Healthy	T2D
acinar cell	112	73
alpha cell	442	443
beta cell	170	99
delta cell	59	54
ductal cell	133	250
gamma cell	75	122

### 5.4.2 Real data results of T2D

Table 5 displays the DEGs identified under various scenarios, with 6, 9, and 38 genes selected, respectively. These DEGs serve as markers for distinguishing healthy individuals from patients with T2D. For instance, a correlation has been observed between the methylation of INS gene promoters and the regulation of INS gene expression in islets and pancreatic  $\beta$  cells [32]. Additionally, [46] discovered that T2D is linked to aberrant pancreatic  $\beta$  cell function, with human  $\beta$  cells expressing elevated levels of HLA-ABC (Class I), CD14/CD9, and HLA-DR (Class II) to a lower extent, as indicated by FACS analysis. Furthermore, [33] proposed that polymorphisms in the CLPS gene could be considered as genetic risk factors for T2D.

This study also compares our method with two others (clr-lasso and coda-lasso). Figure 15 illustrates the overlapping selected genes among the three scenarios using Venn diagrams. Overall, ZIPG-SK consistently identified fewer DEGs compared to the other two methods. Interestingly, as the number of considered cell types decreases from six to two for the selection of DEGs, the number of genes identified by ZIPG-SK increases gradually (from 6 to 38), while the number of genes selected by the other methods decreases progressively (from 64 to 38 and from 64 to 50). This trend is likely due to our method’s ability to address the heterogeneity of multi-source data and identify common DEGs across multiple sources. Consequently, the number of DEGs in  $\alpha$  cells and  $\beta$  cells related to T2D is significantly higher than that in the six cell types. In contrast, the clr-lasso and coda-lasso methods do not effectively address the influence of multiple sources, leading to a decrease in the number of identified DEGs as the number of considered cell types

Table 5: The DEGs identified under various scenarios.

	ZIPG-SK(ZIPG-RF-S)	DEGs	Clr-lasso-CV(overlap)	Coda-lasso-CV(overlap)	Overlap DEGs
6 cell types	6	HLA-AIHLA-BIPTGR1 ACTN4 ZNF331 INS EDN3 VGF IRBP4 SS THLA-BIHLA-AI	47(6)	64(6)	HLA-AIHLA-BIPTGR1 ACTN4 ZNF331 INS
3 cell types	9	SERPINA1 ACTN4 INS PDK4 LAMC2 PPY KRT18 REG1A IRGS2  SPP1 INPY EDN3 MT1G MT2A VGF  CLPS LOXL4 IRBP4 CELA3A CPA2 C15orf48  DDIT3 PNLIP GPX2 PNLIPRP1 MT1X ANXA4  SERPINA1 MT1X TGM2 HLA-AIHLA-BISERPINA1  PTGR1 LDHB ZNF331 KLF10 ATP1A1 CRYBA2  ANXA2 CFI	38(7)	52(8)	EDN3 VGF HLA-BIHLA-AISERPINA1 ACTN4 INS  LAMC2 KRT18 INPY MT2A VGF CLPS  DDIT3 MT1X TGM2 HLA-AIHLA-BISERPINA1  PTGR1 ZNF331 ATP1A1
2 cell types	38		38(16)	50(21)	

decreases. Some DEGs may exhibit variations across the other four cell types while showing no significant differential expression in alpha cells and beta cells.

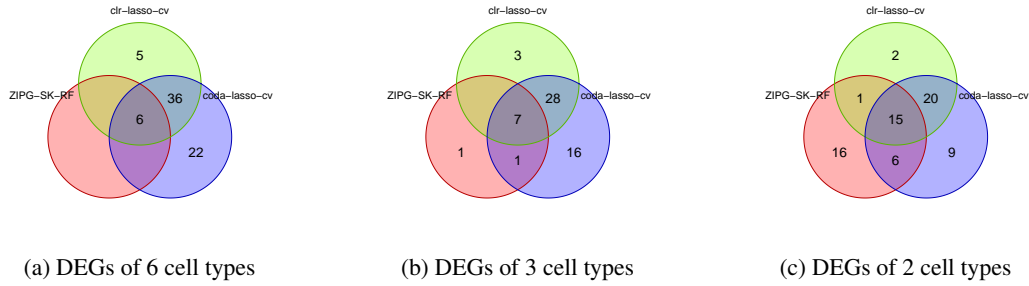


Figure 15: Venn plot of the overlapping selected genes among the three scenarios.

### 5.4.3 Enrichment analysis of T2D

Simultaneously, GO enrichment analysis is conducted on the DEGs identified under various scenarios. Figure 16 displays enriched bubble maps representing the DEGs across these scenarios. The bubble maps primarily highlight the top 10 most enriched functional classes in Biological Processes (BP), Cellular Components (CC), and Molecular Functions (MF). Furthermore, specific gene enrichment analysis results are presented in Table 6. These enriched functions essentially highlight significant distinctions between healthy individuals and those with T2D. Moreover, the enrichment results of the three scenarios exhibits a clear overlapping relationship, wherein the common functional categories of the six cell types are also prominently represented in the enrichment results of the three and two cell types.

In terms of BP, all three cases reveal the crucial role of islet cells in immune regulation, antigen recognition, and stress response. The biological processes involved in all three cases encompass Interferon signaling pathways, antigen processing and presentation of endogenous peptide antigens/exogenous peptide antigens under the MHC I pathway, and protection against immune cell-mediated cytotoxicity. Among these processes, the Interferon signaling pathway may play a key role in regulating immune and inflammatory responses in islets, thereby influencing the stability and function of islet cells [34]. The latter two processes are also associated with inflammation and immunity [35, 47]. With a reduced number of cell types under consideration,  $\alpha$  cells and  $\beta$  cells are more prominently involved in a series of biological processes such as lipid digestion [48] and cellular responses to zinc ions, copper ions, and cadmium ions [49]. Lipid digestion may be linked to glucose homeostasis and insulin signaling pathways, as lipid metabolism is closely associated with these physiological processes [50]. The functional classes of these DEGs are related to inflammatory response and immune regulation, playing a significant role in the pathophysiology of patients with type 2 diabetes, thereby supporting the validity of the above enrichment analysis results.

In terms of CC processes, the three cases all encompass specific functions and regulatory mechanisms in islet tissue structure, cellular communication, and immune regulation. Examples include Extracellular exosome, Golgi membrane, ER to Golgi transport vesicle membrane, and MHC class I protein complex Component. These CC processes may be intricately involved in islet cell communication, signaling, release of extracellular factors, as well as the formation and secretion of insulin-secreting particles [51]. With the reduction of cell types under consideration, the Collagen-containing extracellular matrix in  $\alpha$  cells and  $\beta$  cells, along with CC processes such as the Endosome lumen, Phagocytic vesicle membrane, and Membrane raft, stand out prominently. The DEGs associated with these CC processes may be linked to the matrix structure surrounding the islets and the extracellular environment, potentially influencing the formation of insulin receptor complexes and transmembrane signaling pathways [52, 53].

In terms of MF, all three scenarios involve the role of islet cells in metabolic regulation. For instance, functions such as Signaling receptor binding, Hormone activity, and Peptide antigen binding indicate that these MF functions may involve interactions with insulin receptors or other relevant receptors, potentially being related to the metabolism and regulation of insulin [54, 55]. With a reduction in the number of cell types considered, MF functions in  $\alpha$  cells and  $\beta$  cells also encompass Zinc ion binding and Metal ion binding, suggesting potential associations with metal ion regulation and protein structural stability [56].

In summary, based on the results of DEGs and their enrichment analysis, this method can effectively identify DEGs between healthy individuals and patients with T2D. In comparison to other feature selection methods, the ZIPG-SK method may better address the challenges posed by multi-source heterogeneity, thereby enabling the more effective identification of common features across diverse datasets.

Table 6: Gene enrichment analysis. Examples for specific genes within there celltypes.

	GO term	Representative genes	Term	Adj. P-value
6 cell types	GO:0002479	HLA-BIHLA-A	antigen processing and presentation of exogenous peptide antigen via MHC class I, TAP-dependent	0.0007
	GO:0060333	HLA-BIHLA-A	interferon-gamma-mediated signaling pathway	0.0007
	GO:0000139	HLA-BIHLA-AIINS	Golgi membrane	0.0008
	GO:0070062	HLA-BIHLA-AIPTGR1/ACTN4	extracellular exosome	0.0011
	GO:0005179	INS	hormone activity	0.0225
	GO:0005158	INS	insulin receptor binding	0.0084
3 cell types	GO:0060337	HLA-BIHLA-A	type I interferon signaling pathway	0.0010
	GO:0008284	EDN3/INS	positive regulation of cell population proliferation	0.0111
	GO:0005576	SST/EDN3/SERPINA1/ACTN4/INS	extracellular region	0.0004
	GO:0005783	HLA-BIHLA-A/SERPINA1	endoplasmic reticulum	0.0066
	GO:0005158	INS	insulin receptor binding	0.0110
	GO:0044241	CLPS/PLNLP	lipid digestion	0.0007
2 cell types	GO:0071294	MT2A/MT1F/MT1G/MT1X	cellular response to zinc ion	0.0000
	GO:0045121	ANXA2/ILDH/ATP1A1	membrane raft	0.0130
	GO:0005102	LAMC2/HLA-B/EDN3/INPY/HLA-A	signaling receptor binding	0.0005
	GO:0005179	VGF/EDN3/INPY/PPY	hormone activity	0.0001

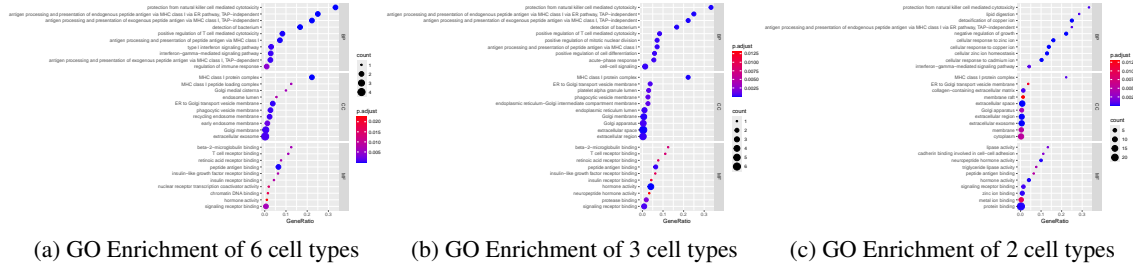


Figure 16: Bubble graphs depicting the top 10 most enriched functional categories across these scenarios. The analysis considers different functional categories, including BP, CC and MF, for each scenarios.